



저작자표시-비영리-변경금지 2.0 대한민국

이용자는 아래의 조건을 따르는 경우에 한하여 자유롭게

- 이 저작물을 복제, 배포, 전송, 전시, 공연 및 방송할 수 있습니다.

다음과 같은 조건을 따라야 합니다:



저작자표시. 귀하는 원저작자를 표시하여야 합니다.



비영리. 귀하는 이 저작물을 영리 목적으로 이용할 수 없습니다.



변경금지. 귀하는 이 저작물을 개작, 변형 또는 가공할 수 없습니다.

- 귀하는, 이 저작물의 재이용이나 배포의 경우, 이 저작물에 적용된 이용허락조건을 명확하게 나타내어야 합니다.
- 저작권자로부터 별도의 허가를 받으면 이러한 조건들은 적용되지 않습니다.

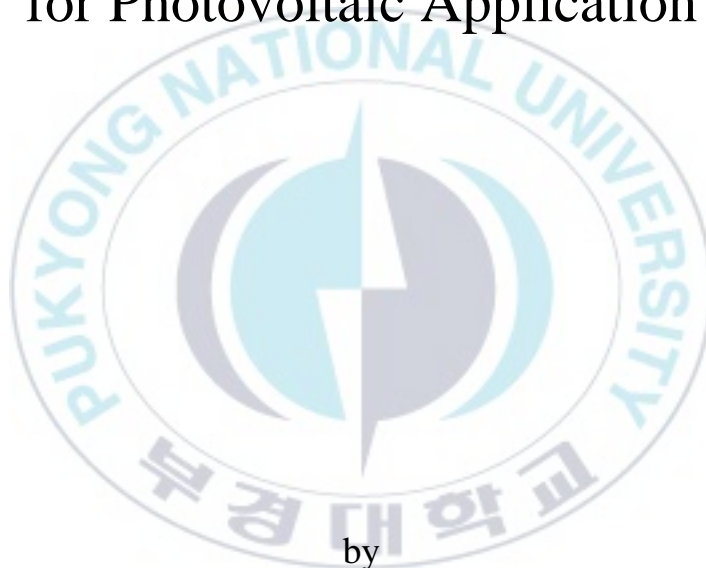
저작권법에 따른 이용자의 권리는 위의 내용에 의하여 영향을 받지 않습니다.

이것은 [이용허락규약\(Legal Code\)](#)을 이해하기 쉽게 요약한 것입니다.

[Disclaimer](#)

Thesis for the Degree of Master of Engineering

Synthesis of Methoxy-substituted
Quinoxaline-based Conjugated Polymers
for Photovoltaic Application



by

Ratri Puspita Wardani
Department of Industrial Chemistry
The Graduate School
Pukyong National University

February, 2021

Synthesis of Methoxy-substituted
Quinoxaline-based Conjugated Polymers for
Photovoltaic Application

(메톡시기를 도입한 귀녹살린 기반의
유기태양 전지용 공액고분자 합성)

Advisor: Prof. Dong Wook Chang

by

Ratri Puspita Wardani

A thesis submitted in partial fulfillment of the requirements
for the degree of
Master of Engineering
in Department of Industrial Chemistry, The Graduate School,
Pukyong National University

February, 2021

**Synthesis of Methoxy-substituted Quinoxaline-based
Conjugated Polymers for Photovoltaic Application**

A dissertation

by

Ratri Puspita Wardani

Approved by:



Prof. Min Young Shon



Prof. Young Eup Jin



Prof. Dong Wook Chang

February 19, 2021

Contents

Contents	i
List of Figures	iii
List of Tables	vi
List of Schemes	vii
Abstract	viii
요약	ix
Chapter I. Introduction	1
I-1. Polymer Solar Cells	1
I-2. Principles of Polymer Solar Cells	3
I-2.1. Light Absorption and Exciton Generation	4
I-2.2. Exciton Diffusion	4
I-2.3. Exciton Dissociation	5
I-2.4. Charge Transport and Collection	5
I-3. Device Structure of Polymer Solar Cells	6
I-4. Parameter of Polymer Solar Cells Device	8
I-4.1. Open Circuit Voltage (V_{oc})	9
I-4.2. Short Circuit Current Density (J_{sc})	10
I-4.3. Fill Factor (FF)	10
I-4.4. Incident Photon to Charge Carrier Efficiency (IPCE)	11
I-5. Molecular Engineering Design of Conjugated Polymers for Solar Cells	11
I-5.1. Low Band-Gap Polymer Solar Cells	12
I-5.2. Polymer Backbone	13
I-5.3. Incorporation of Electron-Donating and Electron-Withdrawing Groups.	16
I-6. The Aim of Thesis	17

Chapter II.	Effect of Electron-withdrawing Fluorine on D- π -A Type Conjugated Polymers for Photovoltaic Application.....	18
II-1.	Experimental Section	18
II-1.1.	Materials and Instruments	18
II-1.2.	Synthesis of Monomers	19
II-1.3.	General Procedure of Polymerization using Stille-Coupling Method with Palladium Catalyst	22
II-1.4.	Fabrication and Analysis of Photovoltaic Devices.....	26
II-2.	Result and Discussion	27
II-2.1.	Synthesis and Physical Properties of Polymers.....	27
II-2.2.	Optical and Electrochemical Properties of Polymers	28
II-2.3.	Photovoltaic Properties of Polymers	33
II-3.	Conclusion	39
Chapter III.	Synthesis of D-A Type Conjugated Polymers for Enhanced Photovoltaic Performance	40
III-1.	Experimental Section	40
III-1.1.	Materials and Instruments	40
III-1.2.	Synthesis of Monomers	41
III-1.3.	General Procedure of Polymerization using Stille-Coupling Method with Palladium Catalyst	42
III-1.4.	Fabrication and Analysis of Photovoltaic Devices.....	45
III-2.	Result and Discussion	46
III-2.1.	Synthesis and Thermal Properties of Polymers.....	46
III-2.2.	Optical and Electrochemical Properties of Polymers	48
III-2.3.	Theoretical Calculations of Polymers	53
III-2.4.	Photovoltaic Properties of Polymers	55
III-3.	Conclusion.....	61
Chapter IV.	Conclusion.....	62
References	63
Acknowledgements	74

List of Figures

Figure I-1.	Mechanism of D-A Type Heterojunction Polymer Solar Cells	3
Figure I-2.	The normal (left) and inverted (right) device configurations with the light source passing through the device from the bottom side. ITO: indium tin oxide; HTL: hole transport layer; AL: active layer; ETL: electron transport layer [23].	8
Figure I-3.	J-V curves in the dark and illuminated polymer solar cells device ..	9
Figure I-4.	Hybridization of molecular orbital energy levels of D-A type copolymer through donor-acceptor intermolecular interactions.....	13
Figure I-5.	IDT unit with various bridging atoms	14
Figure I-6.	The molecule structure of quinoxaline	15
Figure II-1.	Chemical structure of (a) PIDT-QxMT, (b) PIDT-FQxMT, and (c) PIDTT-FQxMT.....	24
Figure II-2.	UV-Visible spectra of polymer in (a) film-state on glass substrate (spectra are offset for clarity) and (b) 1,2-chlorobenzene solution.	29
Figure II-4.	Energy level diagram of all materials in the inverted-type.....	32
Figure II-3.	Cyclic voltammograms of polymers.....	32
Figure II-5.	(a) J-V curve of PSCs under 1.0 sun condition (inset: under the dark condition) and (b) IPCE spectra of PSCs based on PIDT-QxMT, PIDT-FQxMT, and PIDTT-FQxMT.....	34
Figure II-6.	Current density vs. voltage curves of (a) the electron-only and (b) hole-	

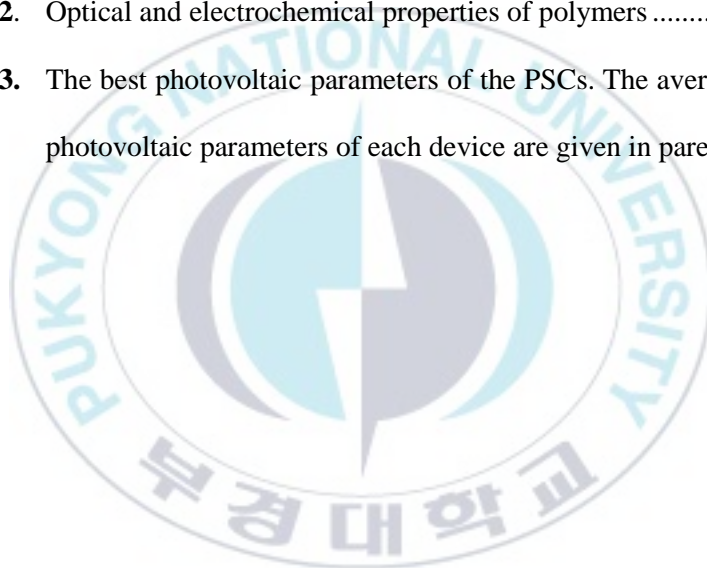
only devices (inset: current density vs. voltage (V)-built-in voltage (V_{bi}) curves with the fitted line)	37
Figure II-7. TEM images of (a) PIDT-QxMT, (b) PIDT-FQxMT, and (c) PIDTT-FQxMT blend film with Y6BO. From left to right, the scale bars are 0.5, 0.2, 0.1 μm , respectively.....	38
Figure III-1. Chemical structure of (a) PIDT-QxM and (b) PIDTT-QxM	43
Figure III-2. TGA curves of PIDT-QxM and PIDTT-QxM at a heating rate of 10°C/min under nitrogen	47
Figure III-3. UV-Visible spectra of polymer in (a) film-state on glass substrate (spectra are offset for clarity) and (b) monochlorobenzene solution	49
Figure III-4. Cyclic voltammograms of polymers	52
Figure III-5. Energy levels of all polymers in an inverted-type PSCs device.....	52
Figure III-6. Frontier molecular orbitals of two-repeating unit models with LUMO and HOMO energy levels calculated at the B3LYP/6-31G** level for (a) PIDT-QxM and (b) PIDTT-QxM	54
Figure III-7. The Simulation of Molar Absorptivity and Oscillator Strength of Polymer	54
Figure III-8. (a) J-V curve of PSCs under 1.0 sun condition (inset: under the dark condition) and (b) IPCE spectra of PSCs based on PIDT-QxM and PIDTT-QxM.	56

- Figure III-9.** Current density vs. voltage curves of (a) the electron-only and (b) hole-only devices (inset: current density vs. voltage (V)-built-in voltage (V_{bi}) curves with the fitted line).....59
- Figure III-10.** TEM images of (a) PIDT-QxM and (b) PIDTT-QxM blend film with Y6BO. From top to bottom, the scale bars are 0.5, 0.2, 0.1 μm , respectively.....60



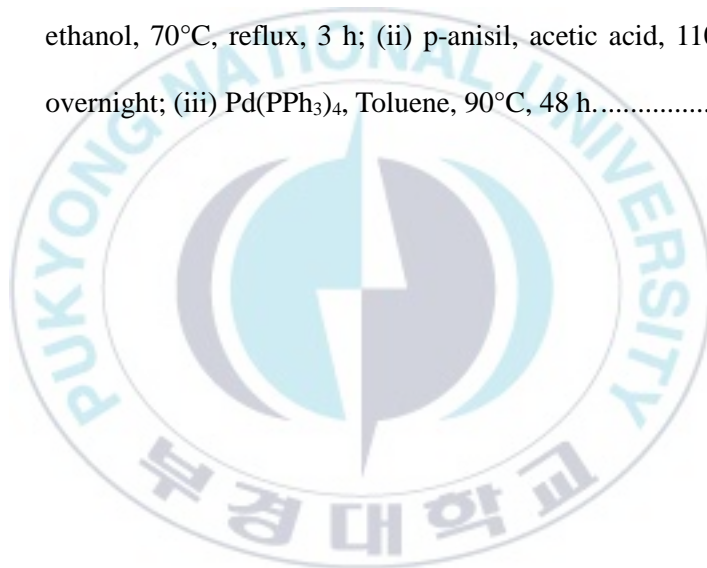
List of Tables

Table II-1.	Molecular weight of the polymers.....	28
Table II-2.	Optical and electrochemical properties of polymers	31
Table II-3.	The best photovoltaic parameters of the PSCs. The averages for the photovoltaic parameters of each device are given in parentheses ..	33
Table III-1.	Molecular weight of the polymers.....	47
Table III-2.	Optical and electrochemical properties of polymers	50
Table III-3.	The best photovoltaic parameters of the PSCs. The averages for the photovoltaic parameters of each device are given in parentheses. .	55



List of Schemes

- Scheme 1.** Synthesis of PIDT-Q_xMT, PIDT-FQ_xMT, and PIDTT-FQ_xMT. (i) Zinc, acetic acid, 80°C, semi-open system; then p-anisil, acetic acid, 110°C, reflux, overnight; (ii) NBs, THF, RT, overnight; (iii) Pd(PPh₃)₄, toluene, 90°C, 48 h25
- Scheme 2.** Synthesis of PIDT-Q_xM and PIDTT-Q_xM. (i) NaBH₄, COCl₂.6H₂O, ethanol, 70°C, reflux, 3 h; (ii) p-anisil, acetic acid, 110°C, reflux, overnight; (iii) Pd(PPh₃)₄, Toluene, 90°C, 48 h.....44



Synthesis of Methoxy-substituted Quinoxaline-based Conjugated Polymers for Photovoltaic Application

Ratri Puspita Wardani

Department of Industrial Chemistry, The Graduate School,
Pukyong National University

Abstract

Two series of methoxy-substituted conjugated polymers based on quinoxaline were successfully synthesized for photovoltaic application. The first series consisted of three polymers where IDT and IDTT were carefully connected to both non-fluorinated and fluorinated 2,3-diphenylquinoxaline (DPQ) through the thiophene bridge to afford **PIDT-QxMT**, **PIDT-FQxMT**, and **PIDTT-FQxMT**, respectively. The best performance fabricated in the inverted device of ITO/ZnO/active layer/MoO₃/Ag was found in **PIDTT-FQxMT** with 8.51% of PCE, 22.23 mA cm⁻² of J_{sc} , 0.72 V of V_{oc} , and 52.4% of FF due to the employment of fluorine substituent and thieno[3,2-b]thiophene units, simultaneously. Another series consisted of two polymers was synthesized by linking IDT and IDTT directly to a simpler DPQ unit to yield **PIDT-QxM** and **PIDTT-QxM**. The best performance was found in **PIDTT-QxM** where the PCE was boosted up to 10.40% with 23.25 mA cm⁻² of J_{sc} , 0.73 V of V_{oc} , and 61.3% of FF ascribed to the expanded conjugation length by the presence of dithieno[3,2-b]thiophene.

메톡시기를 도입한 퀴녹살린 기반의 유기태양 전지용 공액고분자 합성

Ratri Puspita Wardani

부경대학교 대학원 공업화학과

요약

본 연구에서는 두 시리즈의 도너-억셉터 (D-A) 타입 고분자들을 합성한 뒤, 이들을 고분자 기반 유기 태양전지의 광활성층으로 활용하여 광전지 특성을 연구하였다. Indacenodithiophene (IDT) 전자 주계와 메톡시기가 도입된 퀴녹살린 전자 받계에 기초하여 고분자 구조를 설계하였다. 첫 시리즈의 경우, 전자 주계와 전자 받계 사이에 π -bridge가 도입된 PIDT-QxMT, 해당 전자 받계의 퀴녹살린에 불소를 추가 도입한 PIDT-FQxMT 그리고 PIDT-FQxMT의 전자 받계에 IDTT 전자 주계를 결합한 PIDTT-FQxMT를 각각 합성하였다. 첫 시리즈의 광전지 특성은 ITO/ZnO/Active layer/MoO₃/Ag의 배치를 가지는 inverted-type 구조의 소자에서 PIDTT-FQxMT가 불소와 π -bridge의 도입을 통해 최고 효율 8.51%로 관측되었다. 다음으로, IDT와 IDTT의 전자 받계와 메톡시기가 도입된 퀴녹살린의 전자 받계가 직접 연결된 PIDT-QxM과 PIDTT-QxM을 각각 합성하였다. 두번째 시리즈의 광전지 특성의 경우에도 inverted-type 구조의 소자에서 PIDTT-QxM이 공액형 구조의 접합 길이가 늘어남에 따라 최고 효율 10.40%로 관측되었다. 따라서, 이러한 결과는 향후 메톡시기가 도입된 퀴녹살린 기반 공액형 고분자의 구조-물성 간 상관관계 연구에 활용될 수 있을 것이다.

Chapter I. Introduction

I-1. Polymer Solar Cells

Due to the expansion of population and modernization, the energy demand keeps increasing where fossil fuels are expected to contribute 80% out of the total energy supply in 2030 [1]. However, the availability of fossil fuels is limited and the excessive use of fossil fuel attracted global concerns because of the negative impacts given such as climate change, health, and pollution issues [2]. To overcome this problem, people started the use of renewable energy sources as alternative energy [3].

Renewable energy is energy generated from natural resources that emit zero or almost zero emissions such as hydro energy, geothermal energy, biomass energy, wind energy, and solar energy [4]. Among the others, solar energy portrays the greatest source of renewable energy supply. Solar energy can be converted into electricity using photovoltaic (PV) cell which is composed of semiconductor materials.

Recently, the PV cells found in the commercial devices were dominated by inorganic materials [5]. For instance, the crystalline silicon-based PV cells are leading with 27.6% efficiency based on the best research-cell efficiencies by NREL 2020 [6]. However, the technology for semiconductor processing of inorganic material-based solar cells has limitations which are the expensive cost of investment

[7]. Henceforth, there is an urge to develop the new technology which is more economically savvy.

On the other hand, organic solar cells (OSCs) that are mostly polymer solar cells (PSCs) offer various advantages such as plenty of synthetic pathways, tunable molecular structure, the low economical cost in fabrication, light weight, and a wide range of solution processing compared to that inorganic solar cells [7–9]. Moreover, PSCs show significant growth. The PSCs reported in 2001 have 2.5% efficiency [10], along the way, the efficiency increases into 17.4% up to now [6].

With this rapid increase, PSCs considered interesting. Thus, enormous efforts to design and synthesize the new conjugated materials for PSCs are still in progress with the aim to achieve the high efficiency of the organic semiconductor device.

I-2. Principles of Polymer Solar Cells

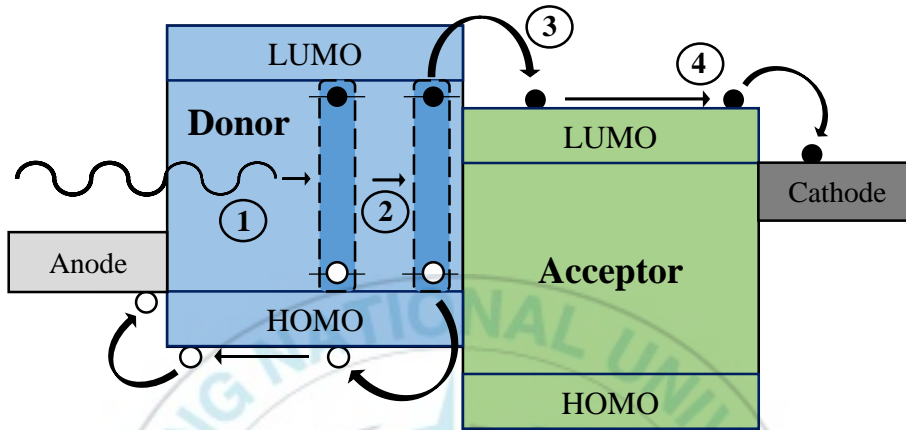


Figure I-1. Mechanism of D-A Type Heterojunction Polymer Solar Cells

Figure I-1 shows the mechanism of the operational principles of polymer solar cells device described in four processes [11–13]: (1) the absorption of a photon in the active layer leading to the formation of excitons (the pair of electron and hole bound); (2) the diffusion of exciton into the donor-acceptor (D-A) interface resulting in the dissociation of exciton into the free electron and hole; (3) the transportation of the free electron from the lowest unoccupied molecular orbital (LUMO) of the donor to the LUMO of the acceptor; and (4) the collection of the free electron and hole to the corresponding electrodes.

I-2.1. Light Absorption and Exciton Generation

As the light absorbed by the donor material through the transparent conducting substrate, the exciton is produced. This occurs because the photon energy absorbed is larger than the band-gap [14]. Unlike inorganic materials that have a large dielectric constant, organic materials typically have a low dielectric constant. Thus, light absorption does not generate the free charge carriers directly. Otherwise, the exciton containing the strong bond of electron and hole pair is generated [15]. This formed exciton requires another step to separate it into the free electron and hole.

I-2.2. Exciton Diffusion

Once the exciton is formed, it diffuses to the donor-acceptor interface through the donor channels. The exciton has a lifetime which is highly correlated with the polymer exciton lengths. Longer exciton lifetime resulted in longer diffusion lengths [16], where the longer exciton diffusion length could contribute to produce more charge carriers [17]. However, the exciton has a short lifetime before it decays. As a result, the exciton diffusion length is limited to the range of 10 nm [18]. Therefore, this parameter is one of the key points affecting organic solar cell design.

I-2.3. Exciton Dissociation

When the exciton reaches the donor-acceptor interface, the exciton dissociates into the free electron and hole. The splitting process happens because of the electrostatic forces at the interface caused by the existence of energy difference between the LUMO of the donor and the LUMO of the acceptor. To maximize the efficient separation of exciton into free electron and holes, the energy level difference between the LUMO of donor and acceptor should be exceeding the exciton binding energy which is in the range of 0.2-0.3 eV depending on the value obtained from the formula below [18].

$$\Delta (\text{LUMO}_D - \text{LUMO}_A) > \text{Exciton binding energy}$$

It is important to choose the proper donor and acceptor to maximize the generation of electric field so it can break the exciton into free charges efficiently [13].

I-2.4. Charge Transport and Collection

After the exciton dissociates into the free electrons and holes, both charges move to the corresponding electrodes, cathode and anode, respectively. The free electrons are acquired by the material with the higher electron affinity, that is the LUMO of the donor, and the free holes are acquired by the material with the lower ionization potential, that is the HOMO of the donor [13]. Thus, the free electrons travel to the cathode through the LUMO of the acceptor channel, while the free holes remain in the donor then collected in the anode [14].

To generate photocurrent, the free electrons and holes must travel from the D-A interface to the corresponding electrodes. These electrodes are connected with the external circuit so the electricity is produced as the result. However, when the charge travels to the electrode, it possibly to recombine or being trapped in a disordered interpenetrating organic material that causes the efficiency drop as the effect [13].

It is found that hole transport has a higher probability of recombination than electron transport. It happens because generally, the hole transport has lower mobility in conducting polymer instead of that the electron transport in the acceptor. The recombination rate is highly correlated with the time needed for the charge carriers to get to the electrodes. In other words, the thicker film will result in a more recombination loss instead of an improvement in the external current [14]. Hence, it is important to increase the hole mobility of the donor to escalate the PSCs device performance.

I-3. Device Structure of Polymer Solar Cells

Recently, there are two types of device structure configuration, which are the normal or conventional type and the inverted type. The normal type consisted of bulk heterojunction (BHJ) layer sandwiched by the transparent metal oxide as the anode in the bottom side and the low work function metal as the cathode in the top side [19].

Bulk heterojunction layer is a blend of donor and acceptor molecules mixture to form a bi-continual layer [20]. The blending of electron donor and electron acceptor would provide the large interfacial area of the active layer, that enhances the PSCs device performance.

It has been verified that the low work function metal such as aluminum will react at the metal-organic interface due to its isotopically labeled oxygen and water. The characteristic of the low work function metal which is reactive affects the degradation mechanism and instability of the device performance [21]. In other words, the low work function metal is not stable to be used in the top electrode because of its sensitivity to the oxygen and the moisture.

The inverted type solar cells have the contrast configuration order compared to the normal type solar cells with metal at the top side functioned as the anode while the cathode is located on the bottom side. In addition, the inverted type commonly uses the high work function metal as the electrode such as Ag that is efficient for the hole collection [19]. Based on studies, the work function of Ag is -4.3 eV. When Ag is exposed to the oxygen, the work function shifted by 0.7 eV into -5.0 eV [22]. To conclude, the oxidation of Ag could maximize the hole collection of the electron donor materials to Ag which later will improve the device performance.

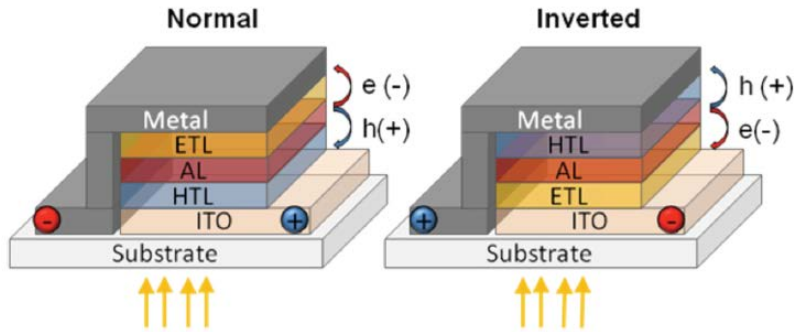


Figure I-2. The normal (left) and inverted (right) device configurations with the light source passing through the device from the bottom side. ITO: indium tin oxide; HTL: hole transport layer; AL: active layer; ETL: electron transport layer [23].

I-4. Parameter of Polymer Solar Cells Device

Power conversion efficiency (PCE) is one of the key points to investigate the performance of polymer solar cells. The value of PCE in percentage is calculated from the formula below.

$$PCE = \frac{V_{oc} \times J_{sc} \times FF}{P_{inc}}$$

Where V_{oc} is the open circuit-voltage with voltage as the unit, J_{sc} is short circuit current with mA/cm^2 as the unit, FF is the fill factor with percent as the unit, and P_{inc} is the incident light power density with mW/cm^2 as the unit.

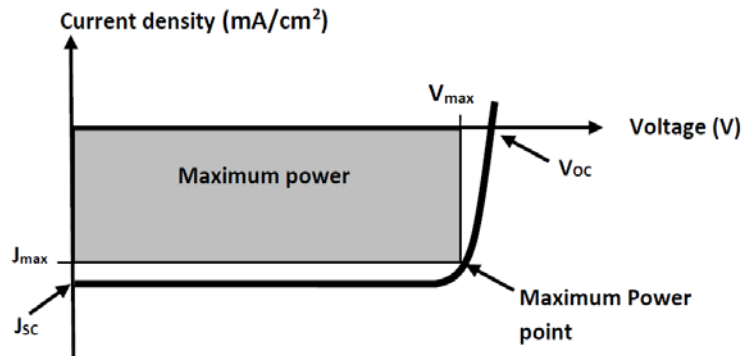


Figure I-3. J-V curves in the dark and illuminated polymer solar cells device

I-4.1. Open Circuit Voltage (V_{oc})

Open circuit voltage (V_{oc}) is the maximum potential produced by the device with the condition that the device is open circuit which means there is no current circulating the circuit [24]. The optimum V_{oc} is approximately the energy gap between the highest occupied molecular orbital (HOMO) level of the donor material and the lowest occupied molecular orbital (LUMO) level of the acceptor material [25]. Lowering the HOMO levels could increase V_{oc} value. However, it is important that the difference between the LUMO of the donor material and the LUMO of the acceptor material should be more than 0.3 eV as the optimum value to keep the exciton dissociation happening for the efficient free charges generation [26].

I-4.2. Short Circuit Current Density (J_{sc})

Short circuit current density (J_{sc}) is the maximum photocurrent density produced by the device with the condition that there is no applied voltage or the open-circuit voltage (V_{oc}) value is zero. This parameter indicates the total quantity of the free charge carriers produced and finally collected to the corresponding electrodes [24]. The short-circuit current densities are often not uniform in a device caused by the low charge carrier lifetime, surface recombination, and the distance to the metal electrode [27]. J_{sc} is equivalent to the spectral absorption area and the absorption intensity toward the active layer. So, the active layer should absorb the broad sunlight to achieve the high J_{sc} value [26].

I-4.3. Fill Factor (FF)

Fill factor (FF) is described as the ratio between the maximum power as the output of organic solar cells device to the J_{sc} and V_{oc} value [24].

It could be expressed in the mathematical formula below.

$$FF = \frac{V_m \times J_m}{V_{oc} \times J_{sc}}$$

where J_m and V_m is the current density and voltage marked at a particular point when the device reached the maximum power, respectively. Referring to the J - V curve in **Figure I.3**, it will form the rectangle shape in the ideal case indicating that the FF value is 100%. The high value of FF correlates with the high number of photo generated carriers produced by the PSCs device [28].

As one of the important parameter in PSCs, the fill factor (FF) indicates the charge generation and collection effectiveness, which is strongly correlated with the properties of the active layer [29]. To improve the active layer morphology, the addition of processing additive and the usage of thermal and solvent annealing process could be done aiming to increase the FF value [30].

I-4.4. Incident Photon to Charge Carrier Efficiency (IPCE)

Incident photon to charge carrier efficiency (IPCE) means the ratio of the total number of the collected carriers and the total number of the incident photons in the active area of the device at a certain wavelength. This parameter shows how efficient the device could convert the incident light into electrical energy [31]. The ideal IPCE value is 100%. On the contrary, the charge recombination happens in the process of exciton separation which will decrease the IPCE value.

I-5. Molecular Engineering Design of Conjugated Polymers for Solar Cells

With the aim to obtain the high performance of bulk heterojunction polymer solar cells device, designing and synthesizing the suitable conjugated polymer is an important factor. The conjugated polymer is expected to have a broad absorption ability and better morphology. The broad absorption ability can be achieved by tuning the bandgap of the energy level of the polymer. While the morphology is highly correlated with the charge carrier mobility. Henceforth, several strategies

have been studied to achieve the high performance of PSCs device.

I-5.1. Low Band-Gap Polymer Solar Cells

Bulk heterojunction (BHJ) active layer in which the electron donor (D) material is blended with the acceptor (A) material is considered an attractive choice for polymer solar cells (PSCs). The molecular design of D/A polymers could affect the optical, electronic, and morphology properties of the material [32].

An effective way to construct the low bandgap polymer is by alternating the electron donor (D) and electron acceptor (A) monomer. This will affect in the induced intermolecular charge across the polymer backbone which resulting in the redistribution of the electron donor and acceptor molecular orbits.

As illustrated in **Figure I-4**, the interaction of the delocalized electrons in each donor and acceptor creates the new molecular orbitals in the D-A interface [33]. This will help to narrow the band-gap through the strong intramolecular interaction between the LUMO-HOMO in the D-A interface. The LUMO is majorly influenced by the acceptor LUMO orbital while the HOMO is highly influenced by the donor HOMO orbital [34].

Semiconducting polymer with 2.0 eV bandgap can absorb photons up to 620 nm which is related to 25% of the total solar energy flux. However, the polymer with approximately 1.1 eV can enlarge the absorption range into 1100 nm which is as same as 77% of the total solar energy [33]. Hence, designing the structure of the D-A conjugated copolymer is developed to obtain the narrow bandgap aiming to

increase the photo-absorption of PSCs.

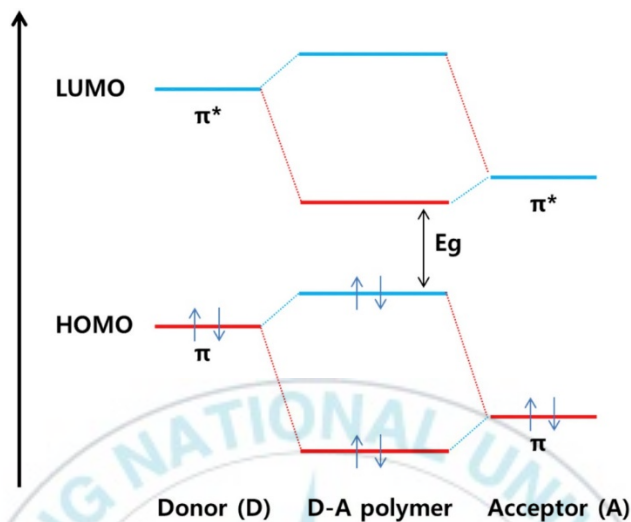


Figure I-4. Hybridization of molecular orbital energy levels of D-A type copolymer through donor-acceptor intermolecular interactions

I-5.2. Polymer Backbone

Among various donors, indacenodithiophene (IDT) is considered promising because of its coplanar fused ring aromatic structure. The three aromatic rings integrated into a single fused molecular structure gives some advantages in which the bridging atom is able to fix the rings coplanarity, maximize the π orbital overlap, and reduce the conformational energetic disorder. Comparing to other donor materials such as 4H-cyclopenta[2,1-b:3,4-b']dithiophene (CPDT), benzo[1,2-b:4,5-b']-dithiophene (BDT), naphthodithiophene (NDTs), the more extended π -conjugated system in the pentacyclic IDT molecules can generate the high photo-physical and electronic properties which are the low degree of energetic disorder

and high carrier mobility [35]. In addition, the integration of the benzene and thiophene into a single fused molecule enhances both J_{sc} and V_{oc} [36,37].

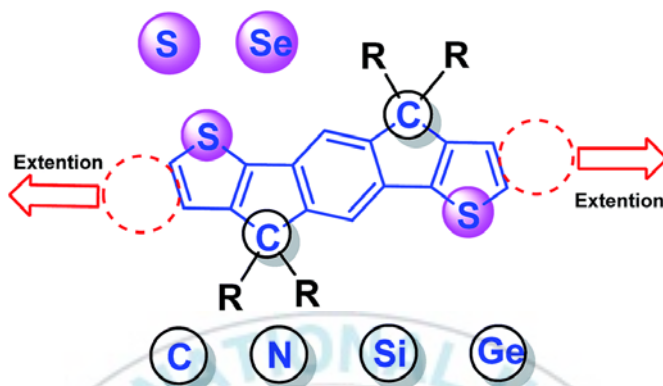


Figure I-5. IDT unit with various bridging atoms

As shown in **Figure I-5**, the bridging atom position also allows the introduction of different side chains such as alkyl or aromatic structure to increase the solubility which later will affect the polymer film morphology [35]. Those features confirm that IDT is a good building block for the polymer backbone. To escalate the performance of the fused-ring polymer, the two thieno[3,2-b]thiophene (TT) units are introduced to the IDT entity replacing the thiophene. As a result, the IDT becomes more extended forming the seven fused-rings namely indacenodithieno[3,2-b]thiophene [38].

Until now, a lot of different acceptors have been reported to synthesize the D-A conjugated polymer. One of the most common acceptors is quinoxaline (Qx) unit. Quinoxaline derivatives is a heterocycle molecule composed of two fused six-elements rings, benzene and pyrazine, with two nitrogen atoms symmetrically

located in one of the rings [39,40].

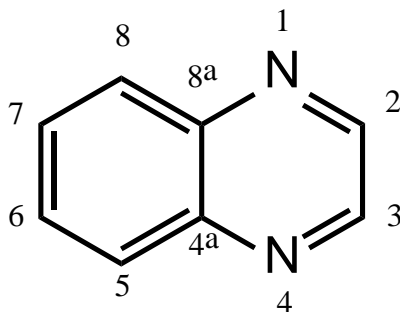


Figure I-6. The molecule structure of quinoxaline

The existence of nitrogen atom assures the quinoxaline as the electron-withdrawing unit. Quinoxaline has several positions that allow the modifications. As shown in **Figure I-6**, some substituents can be incorporated into positions 2, 3, 6, and 7 to extend the vertical conjugation. It can be any chains or functional groups with the properties of electron-withdrawing or electron-donating to occupy the side chains to adjust the solubility and the aggregation tendency of the desired materials.

In addition, quinoxaline monomers is considered as the material with simple synthesis and commonly producing high yield products. The characteristic of easy modification and synthetic procedure offer the advantages to tune the electrochemical properties which further will maximize the PSCs device performance [40].

I-5.3. Incorporation of Electron-Donating and Electron-Withdrawing Groups

Specifically, the incorporation of functional groups such as the electron-donating methyl or methoxy group or electron-withdrawing halogen atoms into the polymer structure is a promising method to enhance the photovoltaic properties of the device performance. The insertion of the functional group also affects the morphology of the polymer. Up to now, there are several studies that analyze the influence of introducing the methoxy group into the polymer structure.

Hou and co-workers studied the impact of the methoxy group position in the structure. It is concluded that the position affects the molecular packing properties, molecular planarity, and intermolecular interactions. The result also showed that certain positions could enhance the exciton dissociation and more balanced charge transport, hence increasing the J_{sc} and FF value in the device [41].

Another study from Zhan'ao Tan and co-workers reported the impact of methoxy group quantity on the structure. The result showed that the visible π - π^* absorption and the photovoltaic properties of the conjugated polymer increase with the increase of the methoxy end group quantity [42].

Fluorine have also attracted a huge interest because of its beneficial features such as the ability to lower both HOMO and LUMO levels, strong aggregation, and high crystallinity [43]. As an example, Putri et. al. introduced the fluorine atoms into the main backbone and the side chain of the quinoxaline. It is reported that the

device performance was improved along with the addition of fluorine units [44].

I-6. The Aim of Thesis

The objective of this thesis is to attain the broad insight of the design and synthesis of the new conjugated polymers and the correlation between the polymer design with its photovoltaic properties applied in the Polymer Solar Cells (PSCs) device. In this study, two series of polymers were synthesized. The first series consisted of three D- π -A type polymers. The polymer was constructed from the IDT derivatives (IDT and IDTT) and methoxy-substituted 2,3-diphenylquinoxaline (DPQ) through a thiophene bridge. The quinoxaline part was modified with fluorine atom in the 6-position for the two, out of the three, polymers. The second series consisted of two polymers with a simpler D-A type. Electron-donating IDT derivatives were carefully linked to the electron-accepting DPQ (QxM). The methoxy group was attached to the phenyl pendants of the DPQ unit.

Chapter II. Effect of Electron-withdrawing Fluorine on D- π -A Type Conjugated Polymers for Photovoltaic Application

II-1. Experimental Section

II-1.1. Materials and Instruments

4,7-di(thiophen-2-yl)benzo[c][1,2,5]thiadiazole (**1**) and 5-fluoro-4,7-di(thiophen-2-yl)benzo[c][1,2,5]thiadiazole (**2**) were synthesized referring to the previously reported literature [45,46]. (4,4,9,9-tetrakis(4-hexylphenyl)-4,9-dihydro-s-indaceno[1,2-b:5,6-b']dithiophene-2,7-diyl)bis(trimethylstannane) (IDT, **7**) and 1,1-[6,6,12,12-tetrakis(4-hexylphenyl)-6,12-dihydrodithieno[2,3-d:2,3-d]-s-indaceno[1,2-b:5,6-b]dithiophene-2,8-diyl]bis[1,1,1-trimethylstannane] (IDTT, **8**) were purchased from Derthon Optoelectronic Materials Science Technology Co., Ltd. All the other chemicals and solvents, unless otherwise specified, were purchased from Sigma-Aldrich and Tokyo Chemical Industry and were used as received. The ^1H , ^{13}C , and ^{19}F nuclear magnetic resonance (NMR) spectra of all the samples were collected using JEOL JNM ECP-400 spectrometer. The ultraviolet-visible (UV-Vis) spectra of all the samples were recorded on Perkin Elmer UV-Vis Lambda 365 Spectrometer. Gel permeation chromatography (GPC) was performed using an Agilent 1200 series instrument with tetrahydrofuran (THF) as an eluent. Cyclic voltammetry (CV) measurements were conducted using a VersaSTAT3 potentiostat

(Princeton Applied Research) with a typical three-electrode system, in which a glassy carbon electrode coated with the samples, a platina wire, and silver wire were used as the working, counter, and reference electrodes, respectively. 0.1 M of tetrabutylammonium hexafluorophosphate solution (Bu_4NPF_6) in acetonitrile was used as the electrolyte solution. Meanwhile, ferrocene/ferrocenium was used as the external standard.

II-1.2. Synthesis of Monomers

II-1.2.1. 2,3-bis(4-methoxyphenyl)-5,8-di(thiophen-2-yl)quinoxaline (3)

4,7-di(thiophen-2-yl)benzo[c][1,2,5]thiadiazole (**1**, 1 mmol) was dissolved in acetic acid and subsequently zinc (20 mmol) was added. The mixture was reacted at 80°C for 5 hr. Then, the mixture was filtered and directly reacted with anisole (1.2 mmol). The solution was reacted overnight. The solution was extracted with ethyl acetate, dried over with MgSO_4 , and filtered, afterwards. The solvent was evaporated in a vacuum condition. The desired product was purified using column chromatography with ethyl acetate/hexane (1/20, v/v) as the eluent. Yield = 81.5% (orange). ^1H NMR (400 MHz, CDCl_3): δ (ppm) = 8.09 (s, 2H), 7.85–7.83 (dd, 2H, $J_1 = 3.8$ Hz, $J_2 = 1.2$ Hz), 7.73–7.71 (m, 4H), 7.51–7.49 (dd, 2H, $J_1 = 5.0$ Hz, $J_2 = 1.2$ Hz), 7.18–7.16 (m, 2H), 6.92–6.9 (m, 4H), 3.85 (s, 6H). ^{13}C NMR (400 MHz, CDCl_3): δ (ppm) = 160.44, 151.3, 138.96, 137.05, 131.98, 131.43, 131.11, 128.86, 126.73,

126.64, 126.3, 113.81, 55.4.

II-1.2.2. 6-fluoro-2,3-bis(4-methoxyphenyl)-5,8-di(thiophen-2-yl)quinoxaline (4)

This material was synthesized using same technique with that is used for monomer **3**. However, 5-fluoro-4,7-di(thiophen-2-yl)benzo[c][1,2,5]thiadiazole (**2**, 1 mmol) was as the starting material. Yield = 92.8%. ¹H NMR (400 MHz, CDCl₃): δ (ppm) = 7.98-7.97 (m, 1H), 7.96-7.93 (d, 1H, J = 7 Hz), 7.85-7.83 (dd, 1H, J₁ = 4.0 Hz, J₂ = 0.8 Hz), 7.72-7.69 (m, 4H), 7.58-7.57 (dd, 1H, J₁ = 5.2 Hz, J₂ = 1.2 Hz), 7.55-7.54 (dd, 1H, J₁ = 5.0 Hz, J₂ = 1.2 Hz), 7.22-7.2 (m, 1H), 7.19-7.17 (m, 1H), 6.93-6.89 (m, 4H), 3.87 (s, 6H). ¹³C NMR (400 MHz, CDCl₃): δ (ppm) = 160.55, 160.43, 160.06, 157.54, 151.75, 150.42, 138.48, 138.39, 137.59, 134.23, 132.07, 131.97, 131.91, 131.16, 131.05, 130.27, 130.13, 129.93, 129.11, 129.08, 126.9, 126.69, 126.47, 116.75, 116.6, 116.45, 113.85, 113.82, 55.4. ¹⁹F NMR (400 MHz, CDCl₃): δ (ppm) = -106.66.

II-1.2.3. 5,8-bis(5-bromothiophen-2-yl)-2,3-bis(4-methoxyphenyl)quinoxaline (5)

2,3-bis(4-methoxyphenyl)-5,8-di(thiophen-2-yl)quinoxaline (**3**, 0.48 mmol) was dissolved in 20 mL of THF. N-bromosuccinimide (1.06 mmol) was added, afterwards. The mixture was reacted with light protection at room temperature overnight. Then, the solvent was removed using vacuum evaporation. The product

was purified using column chromatography with ethyl acetate/hexane (1/20, v/v) as the eluent. Yield = 87.5%. ¹H NMR (400 MHz, CDCl₃): δ (ppm) = 8.03 (s, 2H), 7.69–7.65 (m, 4H), 7.54–7.53 (d, 2H, J = 4.4 Hz), 7.11–7.1 (d, 2H, 3.6 Hz), 6.95–6.91 (m, 4H), 3.86 (s, 6H). ¹³C NMR (400 MHz, CDCl₃): δ (ppm) = 160.48, 151.69, 139.67, 136.36, 131.92, 130.82, 130.3, 129.03, 125.34, 125.25, 116.97, 113.77, 55.33. MALDI-TOF MS: m/z calcd, 663.93; found, 664.58 [M⁺]

II-1.2.4. 5,8-bis(5-bromothiophen-2-yl)-6-fluoro-2,3-bis(4-methoxyphenyl)quinoxaline (6)

This material was synthesized using the same technique with that is used for monomer **5**. However, 6-fluoro-2,3-bis(4-methoxyphenyl)-5,8-di(thiophen-2-yl)quinoxaline (**4**, 0.48 mmol) was used as the starting material. Yield = 87.4%. ¹H NMR (400 MHz, CDCl₃): δ (ppm) = 7.88–7.85 (d, 1H, J = 13.6 Hz), 7.76–7.75 (dd, 1H, J₁ = 4.2 Hz, J₂ = 1.2 Hz), 7.68–7.63 (m, 4H), 7.54–7.53 (d, 1H, J = 4.0 Hz), 7.14–7.11 (m, 2H), 6.95–6.92 (m, 4H), 3.87 (s, 6H). ¹³C NMR (400 MHz, CDCl₃): δ (ppm) = 160.68, 160.53, 159.87, 157.34, 152.03, 150.71, 138.16, 137.62, 137.54, 133.7, 133.44, 132.16, 131.99, 130.92, 130.8, 130.59, 130.47, 130.26, 130.07, 129.07, 125.93, 118.33, 117.76, 116.01, 115.9, 115.2, 114.9, 113.84, 55.43. ¹⁹F NMR (400 MHz, CDCl₃): δ (ppm) = -105.99. MALDI-TOF MS: m/z calcd, 681.92; found, 682.69 [M⁺]

II-1.3. General Procedure of Polymerization using Stille-Coupling Method with Palladium Catalyst

In a schlenk flask, IDT or IDTT monomer (0.20 mmol), dibrominated-quinoxaline monomer (2, 0.20 mmol), and Pd(PPh₃)₄ (3% mol) were dissolved in 10 mL dry toluene. The oxygen was removed by bubbling the solution with nitrogen for 15 minutes. The solution then was stirred at 90°C for 48 hours under nitrogen protection. 2-trimethylstannylthiophene and 2-bromothiophene were used as the end-capping agents aiming to stop the reaction. Both end-capping agents were added to the solution in sequence with 2 hours' interval. After that, the mixture was precipitated in methanol. The solid was collected and purified using Soxhlet extraction with methanol, acetone, hexane, and chloroform, in order. The polymer collected in the chloroform was evaporated until the solution becomes more viscous. The polymer was precipitated in methanol. After that, the purified polymer in the solid form was collected by filtration and dried under vacuum pressure at 70°C overnight.

II-1.3.1. Polymer PIDT-QxMT

(4,4,9,9-tetrakis(4-hexylphenyl)-4,9-dihydro-s-indaceno[1,2-b:5,6-b']dithiophene-2,7-diyl)bis(trimethylstannane) (**7**) and 5,8-bis(5-bromothiophen-2-yl)-2,3-bis(4-methoxyphenyl)quinoxaline (**5**) were used as the monomers. Yield = 92.3% (dark purple solid). ¹H NMR (400 MHz, CDCl₃): δ (ppm) = 8.06 (br, 1H),

7.8-7.76 (br, 6H), 7.43 (br, 1H), 7.4-7.29 (br, 2H), 7.22-7.19 (br, 9H), 7.13-7.11 (br, 7H), 7.08-7.06 (br, 3H), 6.92-6.9 (br, 5H), 3.81 (s, 6H), 2.58-2.56 (br, 8H), 1.6-1.59 (br, 9H), 1.32-1.28 (br, 22H), 0.86-0.84 (br, 13H). Molecular weight (GPC): $M_n = 20.32$ KDa and polydispersity index (PDI) = 2.63.

II-1.3.2. Polymer PIDT-FQ_xMT

(4,4,9,9-tetrakis(4-hexylphenyl)-4,9-dihydro-s-indaceno[1,2-b:5,6-b']dithiophene-2,7-diyl)bis(trimethylstannane) (**7**) and 5,8-bis(5-bromothiophen-2-yl)-6-fluoro-2,3-bis(4-methoxyphenyl)quinoxaline (**6**) were used as the monomers. Yield = 91.18% (dark purple solid). ¹H NMR (400 MHz, CDCl₃): δ (ppm) = 7.94-7.88 (br, 1H), 7.76-7.75 (br, 5H), 7.43-7.29 (br, 3H), 7.22 (br, 8H), 7.16-7.12 (br, 7H), 7.09-6.98 (br, 5H), 6.9 (br, 4H), 3.81-3.76 (m, 6H), 2.58-2.56 (br, 8H), 1.6-1.59 (br, 9H), 1.29-1.28 (br, 22H), 0.85 (br, 13H). Molecular weight (GPC): $M_n = 13.07$ KDa and polydispersity index (PDI) = 2.04.

II-1.3.3. Polymer PIDTT-FQ_xMT

1,1-[6,6,12,12-tetrakis(4-hexylphenyl)-6,12-dihydrodithieno[2,3-d:2,3-d']-s-indaceno[1,2-b:5,6-b']dithiophene-2,8-diyl]bis[1,1,1-trimethylstannane] (**8**) and 5,8-bis(5-bromothiophen-2-yl)-6-fluoro-2,3-bis(4-methoxyphenyl)quinoxaline (**6**) were used as the monomers. Yield = 82.76% (dark purple solid). ¹H NMR (400 MHz, CDCl₃): δ (ppm) = 7.94-7.88 (br, 1H), 7.77-7.75 (br, 5H), 7.52-7.45 (br, 4H), 7.33-7.32 (br, 1H), 7.22-7.07 (br, 18H), 6.94 (br, 4H), 3.85-3.83 (m, 6H), 2.56 (br, 8H), 1.68-1.58 (br, 9H), 1.28-1.24 (br, 22H), 0.85 (br, 13H). Molecular weight (GPC): M_n

= 13.99 KDa and polydispersity index (PDI) = 2.3.

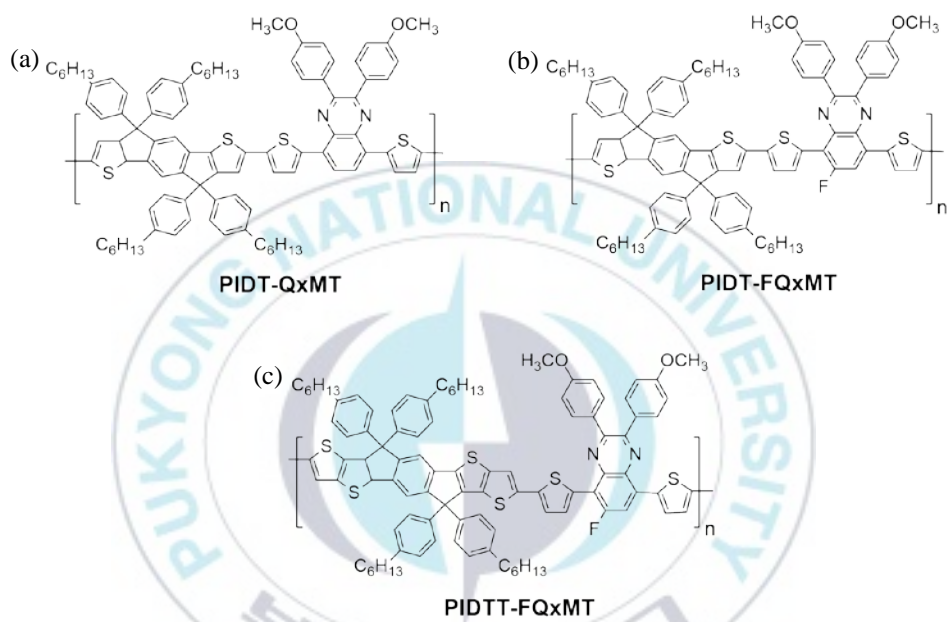
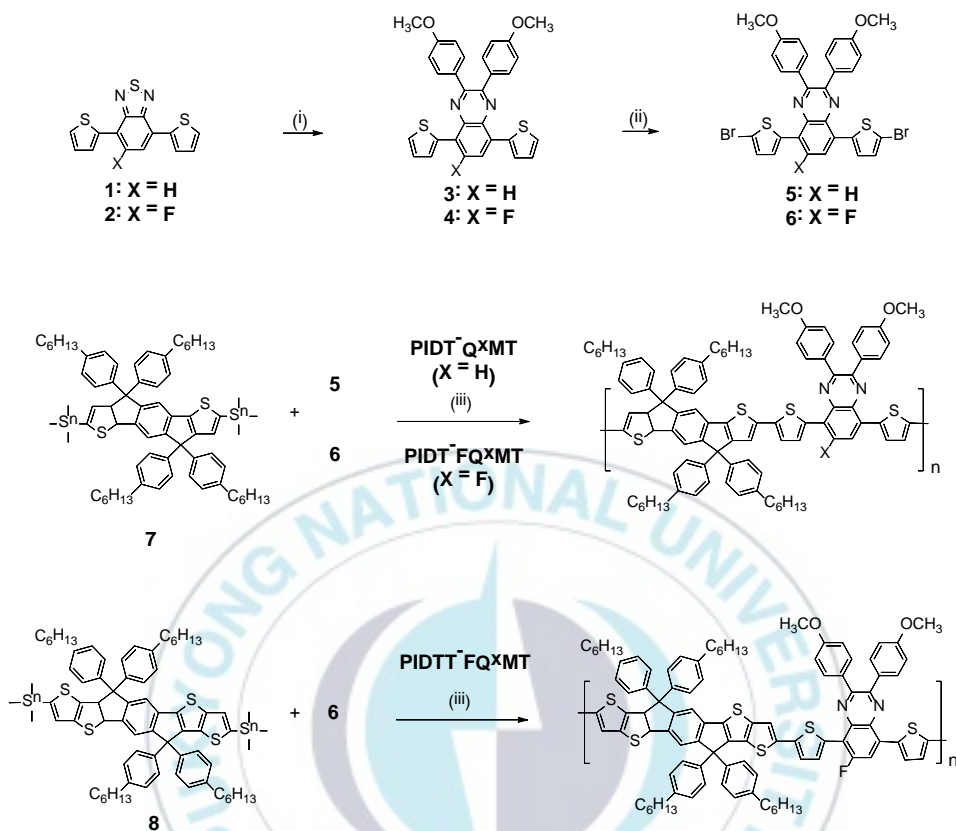


Figure II-1. Chemical structure of (a) PIDT-QxMT, (b) PIDT-FQxMT, and (c) PIDTT-FQxMT.



Scheme 1. Synthesis of PIDT-Q_xMT, PIDT-FQ_xMT, and PIDTT-FQ_xMT. (i) Zinc, acetic acid, 80°C, semi-open system; then p-anisil, acetic acid, 110°C, reflux, overnight; (ii) NBs, THF, RT, overnight; (iii) Pd(PPh₃)₄, toluene, 90°C, 48 h

II-1.4. Fabrication and Analysis of Photovoltaic Devices

The polymer was fabricated on the inverted-type of organic solar cells device. The device structure consisted of ITO/ZnO/active layer/MoO₃/Ag in which the active layer containing of donor polymer and Y6BO acceptor blend. Y6BO was purchased from nano-C, Inc. The fabrication was firstly started by the sol-gel process. Zinc acetate dehydrate (0.164 g) was mixed with ethanolamine (0.05 mL) in 1 mL of methoxyethanol at 60°C for 30 minutes. This step produced ZnO film with 25 nm thickness in which deposited on ITO glass, accordingly. To partially crystallize the ZnO film, the glass was going through thermal curing process at 200°C for 10 minutes. Secondly, the active layer was made by blending the donor polymer with Y6BO acceptor according to each blend ratio. 6 mg of polymer and 12 mg of Y6BO were dissolved in 1 mL of chloroform to give 3:6 blend ratio. While, 6 mg of polymer and 14 mg of Y6BO were dissolved in 1 mL of chloroform to give 3:7 blend ratio. Both blend ratios were added with 0.5% v/v 1,8-diiodooctane (DIO). It was continued by filtration through 0.2 μm polytetrafluoroethylene membrane filter. The blend solution was deposited through spin-coating varying between 1500 to 3000 rpm for 60 seconds to give the uniform active layer thin films with in the range of 105 to 115 nm thickness. The film thickness was measured by Alpha-Step IQ surface profiler (KLA-Tencor Co.). Lastly, MoO₃ and Ag were sequentially deposited on the top of the active layer with 3 nm and 100 nm thickness, respectively, by thermal evaporation through shadow mask with 0.13 cm² device area at 2×10⁻⁶ Torr. The *J-V*

characteristics of the device was investigated by using KEITHLEY Model 400 source-measure unit under the 1.0 sun (100 mW/cm²) condition from 150 W Xe lamp with AM 1.5G filter. The calibration was done by using a Si reference cell with KG5 filter certified by National Institute of Advance Industrial Science and Technology prior to the simulation.

II-2. Result and Discussion

II-2.1. Synthesis and Physical Properties of Polymers

The synthetic route to produce all the monomers and polymers is depicted in Scheme 1. The starting material **1** and **2** were reduced by zinc under acetic acid. This reaction was done in semi-open system for 5 hours and directly filtered to remove the zinc after that. The reaction was continued by a condensation reaction with the α -diketone of 1,2-bis(4-methoxyphenyl)ethane-1,2-dione to produce DPQ monomer **3** and **4**. The monomer **3** and **4** were further reacted through a bromination reaction with N-bromosuccinimide under THF solvent in the room temperature overnight to yield the final monomer **5** and **6**. Eventually, the Stille coupling of IDT derivatives (**7** and **8**) and the DPQ monomer (**5** and **6**) was carefully done to produce the **PIDT-QxMT**, **PIDT-FQxMT**, and **PIDTT-FQxMT**, respectively, as shown in **Figure II-1**. To validate the chemical structure of all materials, some analytical techniques were conducted to the polymers. The three polymers show the good solubility in typical

organic solvents including toluene, THF, and chloroform because of the alkyl and alkoxy chains presence in IDT derivatives and DPQ monomer.

Table II-1. Molecular weight of the polymers

Polymer	M_n (kDa)	M_w (kDa)	PDI
PIDT-QxMT	20.32	45.99	2.26
PIDT-FQxMT	13.07	26.68	2.04
PIDTT-FQxMT	13.99	32.12	2.3

Gel permeation chromatography (GPC) was employed to attain the number-average molecular weights (M_n), weight-average molecular weights (M_w), and polydispersity index (PDI), as presented in **Table II-1**. The M_n and PDI values of polymers are 20.32 kDa and 2.26 for **PIDT-QxMT**, 13.07 kDa and 2.04 for **PIDT-FQxMT**, and 13.99 kDa and 2.3 for **PIDTT-FQxMT**.

II-2.2. Optical and Electrochemical Properties of Polymers

The optical properties of polymers were analyzed through the UV-Visible measurement in the 1,2-chlorobenzene solution and a thin-film. **Figure III-2a,b** showed the two main absorption peaks in the range of 350 to 580 nm correspond to the delocalized π - π^* transition and 600 to 800 nm refer to the intramolecular charge transfer (ICT) along the polymer chain.

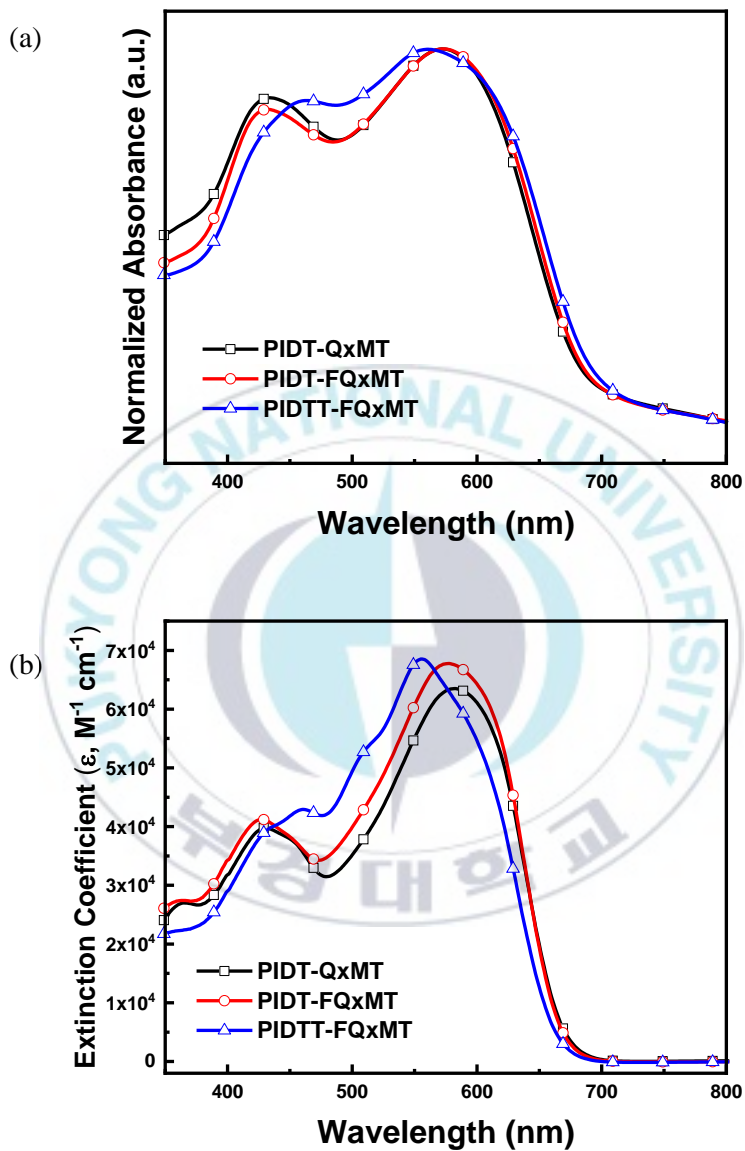


Figure II-2. UV-Visible spectra of polymer in (a) film-state on glass substrate (spectra are offset for clarity) and (b) 1,2-chlorobenzene solution

According to **Figure II-2a**, the maximum absorption in both π - π^* and ICT region of **PIDT-FQxMT** was similar with the reference polymer **PIDT-QxMT** (572 nm). Interestingly, the **PIDTT-FQxMT** exhibited the red-shifted π - π^* absorption region owing to the expanded conjugation length in IDTT-based polymer. The replacement of IDT into IDTT in **PIDTT-FQxMT** increased the distance between polymer chains. The increased distance between donor and acceptor unit resulting in a blue-shifted high wavelength absorption. This result is supported by previous literatures [47,48]. The absorption edge of the fluorinated polymers (**PIDT-FQxMT** and **PIDTT-FQxMT**) was red-shifted than the reference polymer (**PIDT-QxMT**). Accordingly, the calculated optical band-gaps were systematically decrease along with the addition of F-substituent and thieno[3,2-b]thiophene units. In addition, the highest absorption coefficient value was found in **PIDTT-FQxMT** owing to the stronger ICT connection between IDTT and DPQ monomer which was reinforced by F-substituent, as well [44].

To investigate the electrochemical properties of the polymers, cyclic voltammetry (CV) measurement was used. The oxidation onset was attained and the HOMO energy level can be calculated, thereafter. As shown in **Figure II-3**, the HOMO energy level of **PIDT-QxMT**, **PIDT-FQxMT**, and **PIDTT-FQxMT** are -5.06, -5.11, and -5.09 eV, respectively, by using ferrocene as the energy level reference below the vacuum level. The lower HOMO value of fluorinated polymers was due to the influence of electron-withdrawing fluorine unit [44,49–51].

Table II-2. Optical and electrochemical properties of polymers

Polymer	λ_{edge}	$\lambda_{max}^{solution}$	HOMO (eV) ^e	LUMO (eV) ^e
	(nm) ^a ,	(nm) ^c ,		
	E_{gap}^{opt} (eV) ^b	(λ_{max}^{film} (nm) ^d)		
PIDT-QxMT	686, 1.81	430, 582 (435, 572)	-5.06	-3.06
PIDT-FQxMT	688, 1.80	428, 577 (432, 572)	-5.11	-3.13
PIDTT-FQxMT	695, 1.78	461, 556 (466, 557)	-5.09	-3.17

^aAbsorption edge of film, ^bEstimated optical band-gap from λ_{edge} , ^cMaximum wavelength of polymer in chloroform solution, ^dMaximum wavelength of polymer in solid-state, ^eEstimated from the oxidation onset potential.

Nonetheless, **PIDTT-QxMT** possessed a slightly increased HOMO level owing to the utilization of thieno[3,2-b]thiophene as the electron-donating in the polymer structure [52]. As listed in **Table II-2**, the LUMO energy levels were -3.06, -3.13, and -3.17 eV for **PIDT-QxMT**, **PIDT-FQxMT**, and **PIDTT-FQxMT**. This

result indicated that the LUMO levels of the fluorine-modified polymers were lower than the reference polymer .

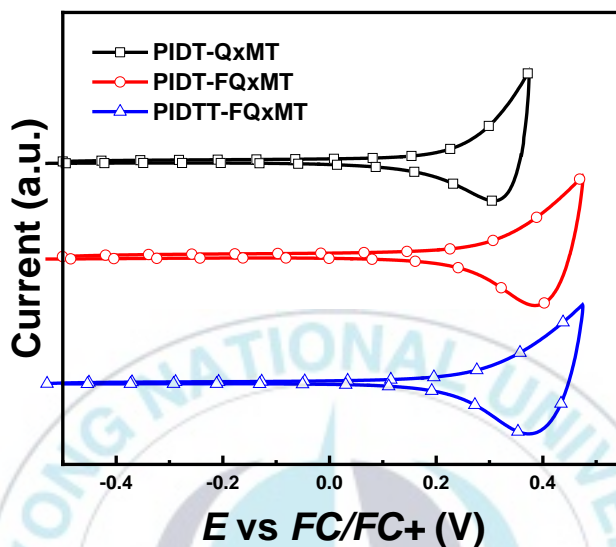


Figure II-4. Cyclic voltammograms of polymers

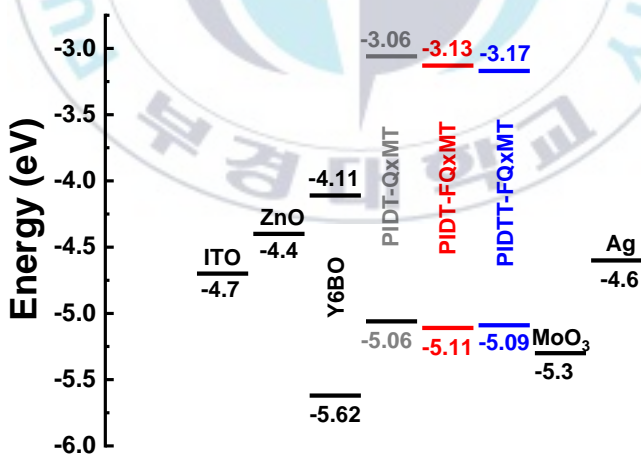


Figure II-3. Energy level diagram of all materials in the inverted-type

II-2.3. Photovoltaic Properties of Polymers

The photovoltaic properties of the polymers were evaluated by constructing an inverted-type PSCs device with ITO (15 Ω)/ZnO (25 nm)/active layer (polymer:Y6BO) (105/115 nm)/MoO₃ (3 nm)/Ag (100 nm) configuration.

Table II-3. The best photovoltaic parameters of the PSCs. The averages for the photovoltaic parameters of each device are given in parentheses

Polymer	J_{sc} (mA cm ⁻²)	V_{oc} (V)	FF (%)	PCE (%)	R_s (Ω cm ²) ^a
PIDT-QxMT	17.18	0.73	51.8	6.50	2.86
	(17.05)	(0.73)	(51.5)	(6.41)	
PIDT-FQxMT	19.92	0.77	51.0	7.82	2.37
	(19.73)	(0.77)	(50.4)	(7.66)	
PIDTT-FQxMT	22.23	0.73	52.4	8.51	2.32
	(22.08)	(0.73)	(51.8)	(8.37)	

^aThe series resistance estimated from the corresponding best device.

The blend ratio of polymer donor and Y6BO acceptor was varied to obtain the maximum device performance. The blend ratio from 3:4 to 3:8 w/w in chloroform solution was made. The best blend ratio was 3:6 for **PIDT-QxMT** and **PIDT-FQxMT**, whereas 3:7 for **PIDTT-FQxMT** with 0.5% v/v of processing additive 1,8-diodooctane (DIO).

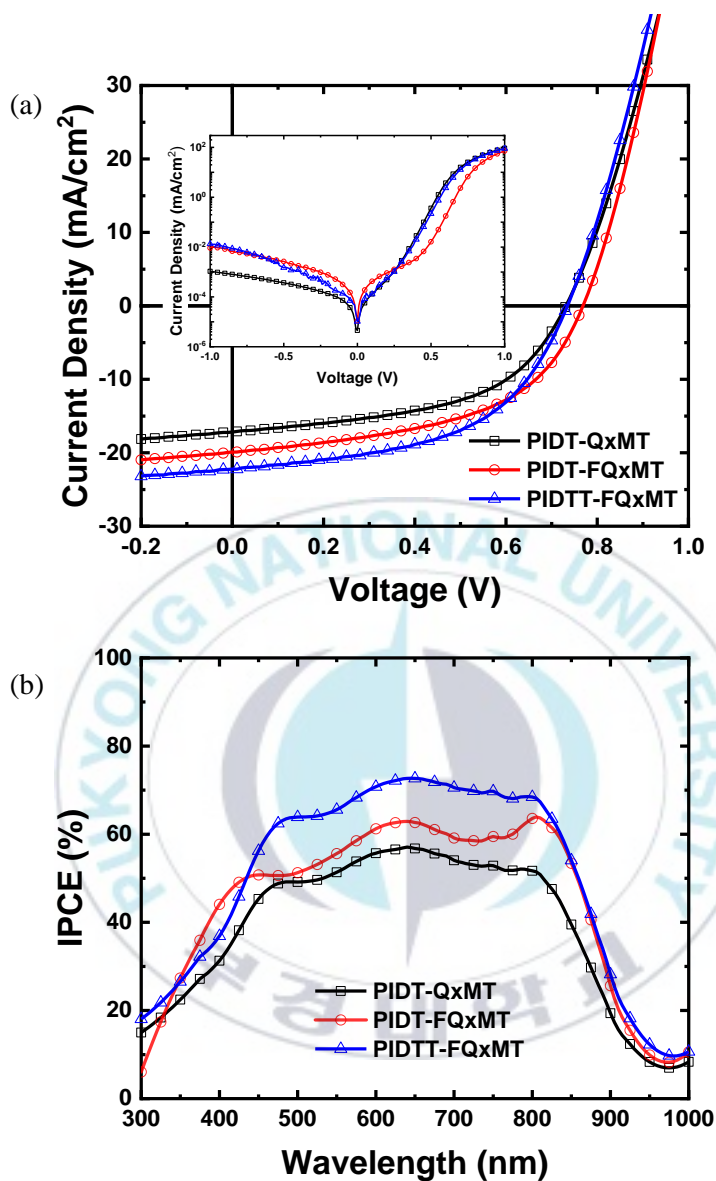


Figure II-5. (a) J-V curve of PSCs under 1.0 sun condition (inset: under the dark condition) and (b) IPCE spectra of PSCs based on PIDT-QxMT, PIDT-FQxMT, and PIDTT-FQxMT.

Figure II-5a expresses the current density vs. voltage (J-V) curves of the PSCs device at its optimized condition under AM 1.5G illumination and the whole photovoltaic properties are listed in **Table II-3**. The PCE of the devices based on the reference polymers **PIDT-QxMT** was limited to 6.50%, while the devices based on the **PIDT-FQxMT** and **PIDTT-FQxMT** were enhanced to 7.82% and 8.51%, consecutively. The apparent increase in PCE of the device based on the fluorinated polymers was corresponding to the gradual improvement of the current circuit density (J_{sc}) with the value of 17.18, 19.92, 22.23 mA cm⁻² following the order of **PIDT-QxMT**, **PIDT-FQxMT**, and **PIDTT-FQxMT**. This result is coherent with the trend in molar extinction coefficient. Furthermore, the open-circuit voltage (V_{oc}) of **PIDT-FQxMT** (0.77 V) was higher than the reference polymer **PIDT-QxMT** (0.73 V), as the result of the electron-withdrawing contribution of fluorine. In contrast, the device based on **PIDTT-FQxMT** (0.73 V) exhibited the lower V_{oc} compared to that **PIDT-FQxMT**, (0.77 V) in which perfectly matched with the trend in HOMO levels. Additionally, all polymers showed the similar value of fill factor (FF) ranging around 51.0-52.4%.

Figure II-5b pointed that all polymers possessed the broad light absorption in the wavelength range of 350 to 900 nm with the maximum incident photon-to-current efficiency (IPCE) value around 70%. This result validates the trend in J_{sc} value. The inset in **Figure II-5a** shows the J-V curves under the darkness to gain the series resistance (R_s) values. The R_s values were 2.86, 2.37, and 2.32 Ω cm²

decreasing in the order of **PIDT-QxMT**, **PIDT-FQxMT**, and **PIDTT-FQxMT**, which is consistent with the overall photovoltaic properties of the devices.

The charge-transport properties of all polymers were analyzed by constructing two devices with different order, ITO/ZnO/active layer/LiF/Al for the electron-only device and ITO/PEDOT:PSS/active layer/Au for the hole-only device. As depicted in **Figure II-6**, the three polymers show the characteristic of space-charge-limited-current (SCLC) which is expressed in the famous Mott-Gurney equation [53,54]. The hole mobilities were calculated to be 5.45×10^{-4} , 6.04×10^{-4} , and $9.44 \times 10^{-4} \text{ cm}^2 \text{ V}^{-1} \text{ s}^{-1}$, whereas the electron mobilities were 1.07×10^{-3} , 1.13×10^{-3} , and $1.88 \times 10^{-3} \text{ cm}^2 \text{ V}^{-1} \text{ s}^{-1}$ for **PIDT-QxMT**, **PIDT-FQxMT**, and **PIDTT-FQxMT**, respectively. It can be deduced that the incorporation of F-substituent could enhance the charge mobilities, then, the device performance was significantly improved.

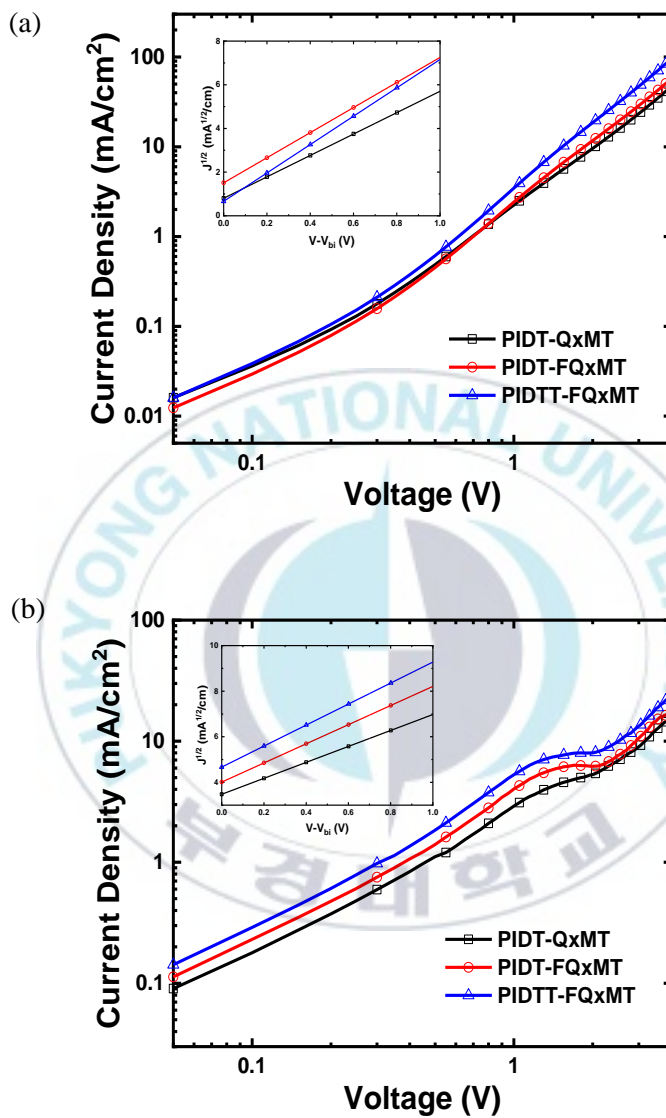


Figure II-6. Current density vs. voltage curves of (a) the electron-only and (b) hole-only devices (inset: current density vs. voltage (V)-built-in voltage (V_{bi}) curves with the fitted line)

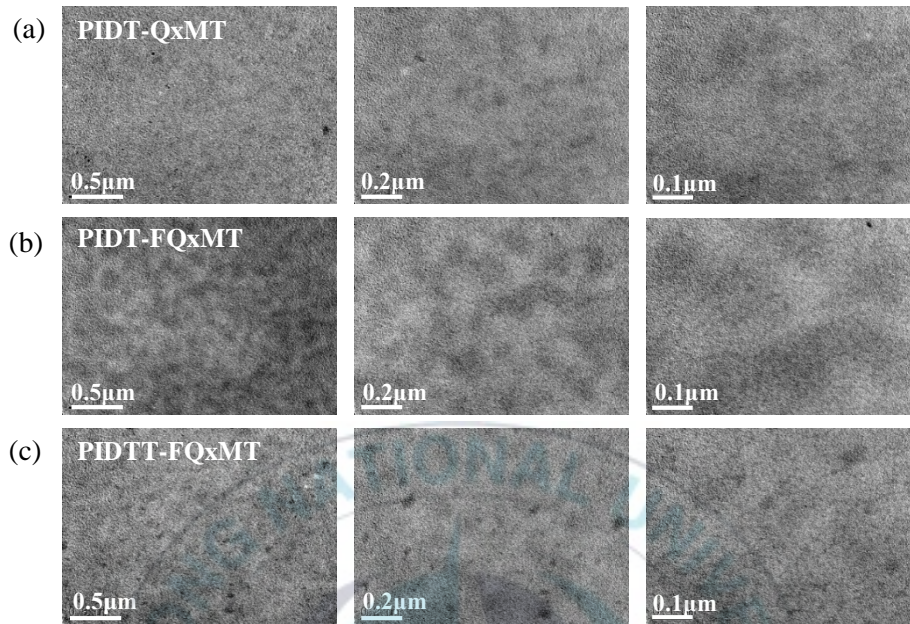


Figure II-7. TEM images of (a) PIDT-QxMT, (b) PIDT-FQxMT, and (c) PIDTT-FQxMT blend film with Y6BO. From left to right, the scale bars are 0.5, 0.2, 0.1 μm , respectively.

Figure II-7 explained the morphology of polymer/Y6BO blend film which was measured by transmission electron microscopy (TEM). **PIDTT-FQxMT** owned the best microscale phase separation, while the worst one was found in **PIDT-FQxMT**. The morphological result was coherent with the trend in *FF* values.

II-3. Conclusion

Three new D- π -A type conjugated polymers were synthesized via Stille coupling reaction. The electron-donating IDT was connected to a methoxy-substituted quinoxaline to produce the reference polymer **PIDT-QxMT**. Then, the electron-withdrawing fluorine unit was introduced into the quinoxaline. IDTT and IDTT were selectively connected to the F-modified DPQ to afford **PIDT-FQxMT** and **PIDTT-FQxMT**, respectively. These polymers were blended with the Y6BO acceptor in the active layer of the inverted-type PSCs. The PCE based on the fabricated device was 6.50%, 7.82%, and 8.51% for **PIDT-QxMT**, **PIDT-FQxMT**, and **PIDTT-FQxMT**, respectively. The best device performance was found in **PIDTT-FQxMT** owing to the electron-withdrawing effect of F atom and the more planar structure caused by the thieno[3,2-b]thiophene units. The introduction of fluorine decreased the HOMO level which further affect the V_{oc} value. The similar value of FF was observed. Interestingly, the J_{sc} value was improved in the order of **PIDT-QxMT**, **PIDT-FQxMT**, and **PIDTT-FQxMT** indicating the excellent charge generation of the devices. The best morphology was seen in **PIDTT-FQxMT** blend film showing the good charge separation, thus confirming the improvement in J_{sc} value. Overall, this study provides the significant effect of the fluorine-modified conjugated polymers. A deeper study is needed to improve the photovoltaic parameters for the better device performance.

Chapter III. Synthesis of D-A Type Conjugated Polymers for Enhanced Photovoltaic Performance

III-1. Experimental Section

III-1.1. Materials and Instruments

(4,4,9,9-tetrakis(4-hexylphenyl)-4,9-dihydro-s-indaceno[1,2-b:5,6-b']dithiophene-2,7-diyl)bis(trimethylstannane) (IDT, **3**) and 1,1-[6,6,12,12-tetrakis(4-hexylphenyl)-6,12-dihydrodithieno[2,3-d:2,3-d]-s-indaceno[1,2-b:5,6-b']dithiophene-2,8-diyl]bis[1,1,1-trimethylstannane] (IDTT, **4**) were purchased from Derthon Optoelectronic Materials Science Technology Co., Ltd. All the other chemicals and solvents, unless otherwise specified, were purchased from Sigma-Aldrich and Tokyo Chemical Industry and were used as received. The ^1H and ^{13}C nuclear magnetic resonance (NMR) spectra of all the samples were collected using JEOL JNM ECP-600 spectrometer and JEOL JNM ECP-400 spectrometer. The ultraviolet-visible (UV-Vis) spectra of all the samples were recorded on Perkin Elmer UV-Vis Lambda 365 Spectrometer. Gel permeation chromatography (GPC) was performed using an Agilent 1200 series instrument with tetrahydrofuran (THF) as an eluent. Cyclic voltammetry (CV) measurements were conducted using a VersaSTAT3 potentiostat (Princeton Applied Research) with a typical three-electrode system, in which a glassy carbon electrode coated with the samples, a platina wire,

and silver wire were used as the working, counter, and reference electrodes, respectively. 0.1 M of tetrabutylammonium hexafluorophosphate solution (Bu_4NPF_6) in acetonitrile was used as the electrolyte solution. Meanwhile, ferrocene/ferrocenium was used as the external standard.

III-1.2. Synthesis of Monomers

5,8-dibromo-2,3-bis(4-methoxyphenyl)quinoxaline (2)

In a round-bottom flask, 4,7-dibromobenzo[c][1,2,5]thiadiazole (1 mmol) was dissolved in ethanol. NaBH_4 (18.88 mmol) and $\text{COCl}_2 \cdot 6\text{H}_2\text{O}$ (0.1 mmol) were added and the mixture was reacted at 70°C for 3 hr. After that, the mixture was filtered to remove $\text{COCl}_2 \cdot 6\text{H}_2\text{O}$ and then poured into water. The solution was extracted with ether, dried over with MgSO_4 , and filtered. The solvent was evaporated and the crude product was directly reacted with anisole (1.2 mmol). The solution was refluxed overnight. In the next day, the solution was extracted with ethyl acetate, dried over with MgSO_4 , and filtered. The solvent was evaporated in vacuum condition. The product was purified using column chromatography with ethyl acetate/hexane (1/20, v/v) as the eluent. Yield = 74% (white). ^1H NMR (400 MHz, CDCl_3): δ (ppm) = 7.86 (s, 2H), 7.68–7.65 (m, 4H), 6.92–6.88 (m, 4H), 3.85 (s, 6H). ^{13}C NMR (400 MHz, CDCl_3): δ (ppm) = 160.82, 153.46, 138.99, 132.52, 131.67, 130.53, 123.42, 113.83, 55.31. GC-MS: m/z calcd, 499.96; found, 500.05 [M^+].

III-1.3. General Procedure of Polymerization using Stille-Coupling Method with Palladium Catalyst

In a schlenk flask, IDT or IDTT monomer (0.20 mmol), dibrominated-quinoxaline monomer (**2**, 0.20 mmol), and Pd(PPh₃)₄ (3% mol) were dissolved in 10 mL dry toluene. The oxygen was removed by bubbling the solution with nitrogen for 15 minutes. The solution then was stirred at 90°C for 48 hours under nitrogen protection. 2-trimethylstannylthiophene and 2-bromothiophene were used as the end-capping agents aiming to stop the reaction. Both end-capping agents were added to the solution in sequence with 2 hours' interval. After that, the mixture was precipitated in methanol. The solid was collected and purified using Soxhlet extraction with methanol, acetone, hexane, and chloroform, in order. The polymer collected in the chloroform was evaporated until the solution becomes more viscous. The polymer was precipitated in methanol. After that, the purified polymer in the solid form was collected by filtration and dried under vacuum pressure at 70°C overnight.

III-1.3.1. Polymer PIDT-QxM

(4,4,9,9-tetrakis(4-hexylphenyl)-4,9-dihydro-s-indaceno[1,2-b:5,6-b']dithiophene-2,7-diyl)bis(trimethylstannane) (**3**) and 5,8-dibromo-2,3-bis(4-methoxyphenyl)quinoxaline (**2**) were used as the monomers. Yield = 81.66% (dark blue solid). ¹H NMR (600 MHz, CDCl₃): δ (ppm) = 7.96-7.87 (br, 3H), 7.72-7.7 (d,

5H), 7.52 (s, 2H), 7.31-7.29 (br, 7H), 7.12-7.1 (br, 8H), 6.92-6.89 (d, 5H), 3.89 (s, 6H), 2.58 (s, 8H), 1.6-1.59 (br, 8H), 1.34-1.28 (br, 21H), 0.87-0.84 (br, 15H). Molecular weight (GPC): $M_n = 30.02$ KDa and polydispersity index (PDI) = 2.29.

III-1.3.2. Polymer PIDTT-QxM

1,1-[6,6,12,12-tetrakis(4-hexylphenyl)-6,12-dihydrodithieno[2,3-d:2,3-d]-s-indaceno[1,2-b:5,6-b]dithiophene-2,8-diyl]bis[1,1,1-trimethylstannane] (**4**) and 5,8-dibromo-2,3-bis(4-methoxyphenyl)quinoxaline (**2**) were utilized as the monomers. Yield = 76.29% (dark blue solid). $^1\text{H NMR}$ (400 MHz, CDCl_3): δ (ppm) = 8.1-8.04 (br, 2H), 7.74-7.72 (br, 6H), 7.63-7.5 (br, 4H), 7.29-7.28 (br, 6H), 7.09-7.04 (br, 7H), 6.77-6.75 (br, 5H), 3.84 (s, 6H), 2.55 (br, 8H), 1.57 (br, 9H), 1.25-1.24 (br, 22H), 0.83 (13H). Molecular weight (GPC): $M_n = 34.85$ KDa and polydispersity index (PDI) = 3.1.

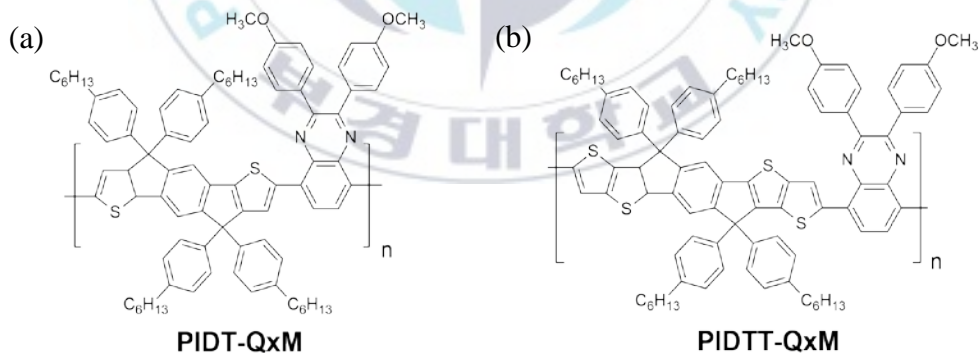
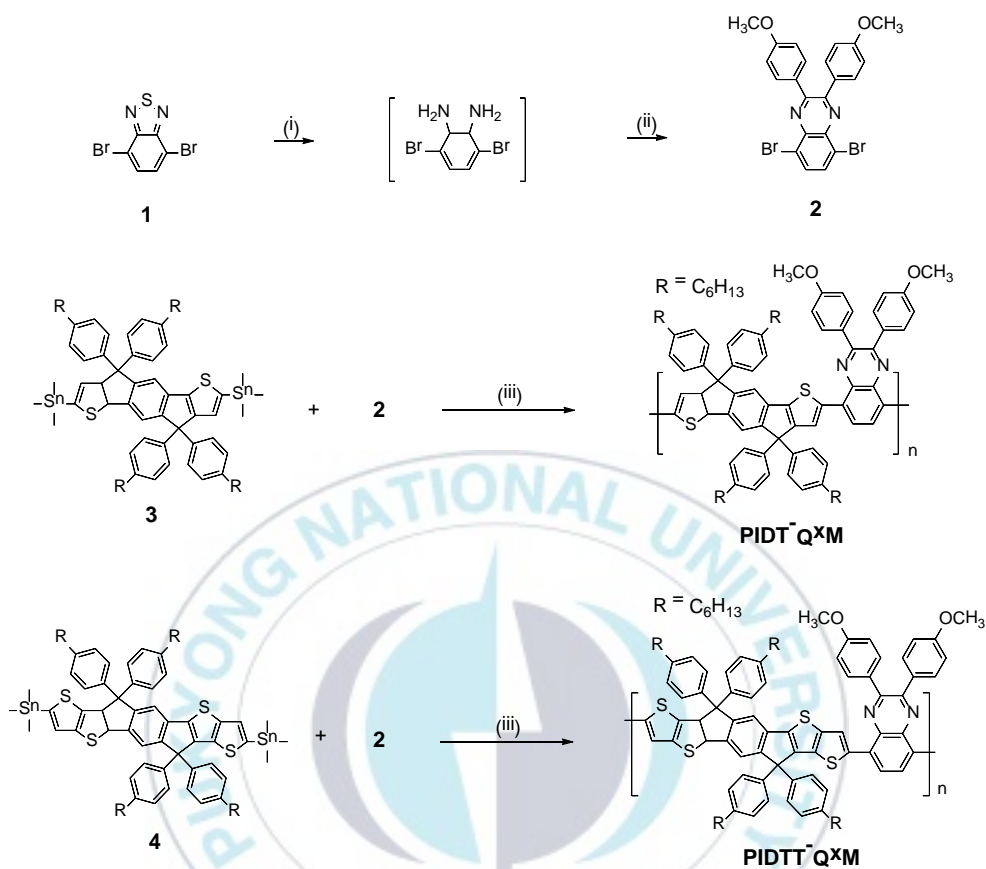


Figure III-1. Chemical structure of (a) PIDT-QxM and (b) PIDTT-QxM



Scheme 2. Synthesis of PIDT-QxM and PIDTT-QxM. (i) $NaBH_4$, $COCl_2 \cdot 6H_2O$, ethanol, $70^\circ C$, reflux, 3 h; (ii) p-anisil, acetic acid, $110^\circ C$, reflux, overnight; (iii) $Pd(PPh_3)_4$, Toluene, $90^\circ C$, 48 h.

III-1.4. Fabrication and Analysis of Photovoltaic Devices

The polymer was fabricated on the inverted-type of organic solar cells device. The device structure consisted of ITO/ZnO/active layer/MoO₃/Ag in which the active layer containing of donor polymer and Y6BO acceptor blend. Y6BO was purchased from nano-C, Inc. The fabrication was firstly started by the sol-gel process. Zinc acetate dehydrate (0.164 g) was mixed with ethanolamine (0.05 mL) in 1 mL of methoxyethanol at 60°C for 30 minutes. This step produced ZnO film with 25 nm thickness in which deposited on ITO glass, accordingly. To partially crystallize the ZnO film, the glass was going through thermal curing process at 200°C for 10 minutes. Secondly, the active layer was made by blending the donor polymer with Y6BO acceptor according to each blend ratio. 6 mg of polymer and 12 mg of Y6BO were dissolved in 1 mL of chloroform to give 3:6 blend ratio. While, 6 mg of polymer and 14 mg of Y6BO were dissolved in 1 mL of chloroform to give 3:7 blend ratio. Both blend ratios were added with 0.5% v/v 1,8-diiodooctane (DIO). It was continued by filtration through 0.2 μm polytetrafluoroethylene membrane filter. The blend solution was deposited through spin-coating varying between 1500 to 3000 rpm for 60 seconds to give the uniform active layer thin films with in the range of 105 to 115 nm thickness. The film thickness was measured by Alpha-Step IQ surface profiler (KLA-Tencor Co.). Lastly, MoO₃ and Ag were sequentially deposited on the top of the active layer with 3 nm and 100 nm thickness, respectively, by thermal evaporation through shadow mask with 0.13 cm² device area at 2×10⁻⁶ Torr. The *J-V*

characteristics of the device was investigated by using KEITHLEY Model 400 source-measure unit under the 1.0 sun (100 mW/cm^2) condition from 150 W Xe lamp with AM 1.5G filter. The calibration was done by using a Si reference cell with KG5 filter certified by National Institute of Advance Industrial Science and Technology prior to the simulation.

III-2. Result and Discussion

III-2.1. Synthesis and Thermal Properties of Polymers

The synthetic route to produce the monomer and polymers is shown in **Scheme 2**. The starting material **1** was reduced by NaBH_4 with the help of $\text{CoCl}_2 \cdot 6\text{H}_2\text{O}$ catalyst under ethanol as the solvent. This reaction was done in reflux condition for 3 hours to yield the intermediate structure. After the extraction process, the intermediate then was condensed with the α -diketone of 1,2-bis(4-methoxyphenyl)ethane-1,2-dione to produce quinoxaline-based monomer **2**. The monomer **2** is the final monomer which will be continued to polymerization using Stille coupling reaction, afterwards. The indacenodithiophene (IDT, **3**) and indacenodithienothiophene (IDTT, **4**) were used as the electron-donating material reacted using the Stille coupling reaction with monomer **2** to construct D-A type conjugated polymers yielding **PIDT-QxM** and **PIDTT-QxM**, respectively, as displayed in **Figure II-1**. To confirm the chemical structure of the synthesized

materials, several analytical techniques were employed to the materials. The two polymers show the good solubility in common organic solvents including toluene, THF, and chloroform because of the alkyl and alkoxy chains existence in IDT derivatives and DPQ monomer.

Table III-1. Molecular weight of the polymers

Polymer	M_n (kDa)	M_w (kDa)	PDI
PIDT-QxM	30.02	68.65	2.29
PIDTT-QxM	34.85	108.06	3.1

To obtain the number-average molecular weights (M_n), weight-average molecular weights (M_w), and polydispersity index (PDI), the gel permeation chromatography (GPC) was employed. The M_n and PDI values of polymers are 30.02 kDa and 2.29 for **PIDT-QxM** and 34.85 kDa and 3.1 for **PIDTT-QxM**.

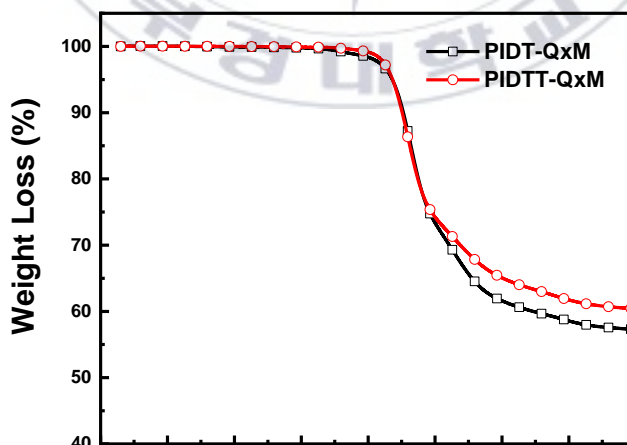


Figure III-2. TGA curves of PIDT-QxM and PIDTT-QxM at a heating rate of 10°C/min under nitrogen

To evaluate the thermal properties of polymers, the thermogravimetric analysis (TGA) was employed with the condition of 10°C/min heating rate under nitrogen atmosphere. All polymers show the good thermal stability indicated by the high decomposition temperature onset with 5% weight loss ($T_{d5\%}$) at 436°C for both **PIDT-QxM** and **PIDTT-QxM**. The TGA curves are shown in **Figure III-2**.

III-2.2. Optical and Electrochemical Properties of Polymers

The optical properties of polymers were measured by conducting the UV-Visible measurement in both chloroform and film-state of the polymers. As presented in **Figure III-2a,b**, the polymers show two main absorption peaks which is a typical characteristic of D-A type polymer. The high absorption band in the range of 300 to 500 nm is refer to the π - π^* transition of the conjugated polymer backbone, while the other high-lying absorption band in the range of 500 to 800 nm refers to the intramolecular charge transfer (ICT) from the donor (IDT derivatives) to the acceptor (quinoxaline) unit [55].

According to **Figure III-3**, **PIDTT-QxM** is more bathochromic-shifted than **PIDT-QxM**. This is attributed to the more planar and extended conjugation length which increases the number of delocalized electrons of **PIDTT-QxM** rather than that **PIDT-QxM**. This result agrees with the previous report [38,56,57]. Moreover, the polymer with IDTT donor exhibited the higher absorption coefficient value than the one with IDT donor owing to the intense ICT connection between IDTT and DPQ

monomer.

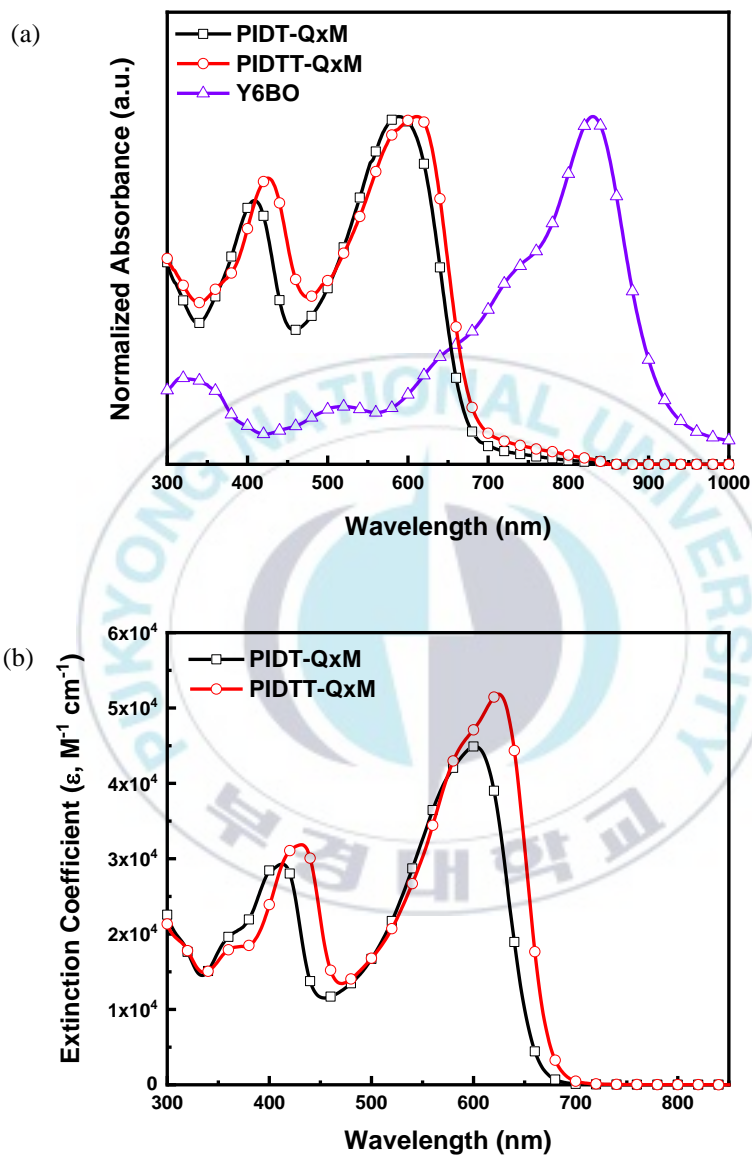


Figure III-3. UV-Visible spectra of polymer in (a) film-state on glass substrate (spectra are offset for clarity) and (b) monochlorobenzene solution

As stated in **Table III-2**, the maximum wavelength absorptions in ICT region with chloroform solution of **PIDT-QxM** and **PIDTT-QxM** are 601 and 625 nm, while the maximum absorptions in solid-state are 589 and 611 nm, respectively. The wavelength onset in solid-state for **PIDT-QxM** and **PIDTT-QxM** are 684 and 690 nm. From this value, the optical band-gap can be calculated resulting in a slightly lower band-gap of **PIDTT-QxM** which is 1.80 eV than **PIDT-QxM** which is 1.81 eV.

Table III-2. Optical and electrochemical properties of polymers

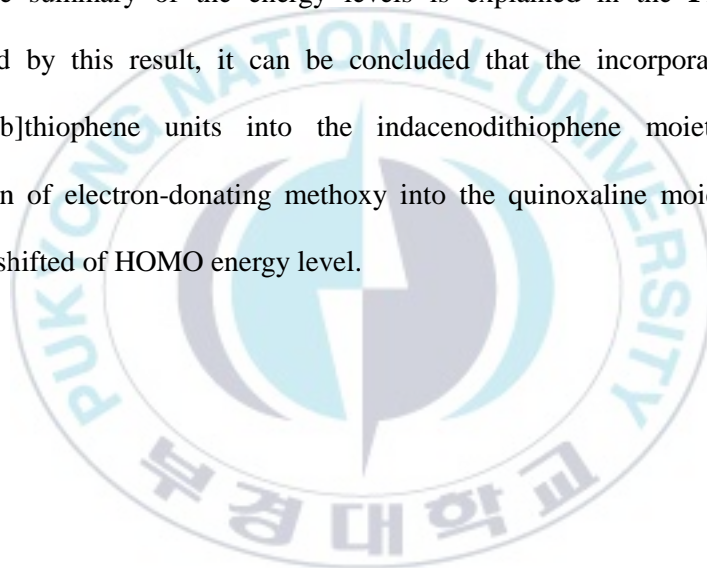
Polymer	λ_{edge}	$\lambda_{max}^{solution}$	HOMO (eV) ^e	LUMO (eV) ^f	E_{gap}^{CV} (eV)
	(nm) ^a ,	(nm) ^c ,			
	E_{gap}^{opt} (eV) ^b	(λ_{max}^{film} (nm) ^d)			
PIDT-QxM	684, 1.81	601 (589)	-5.18	-3.15	2.03
PIDTT-QxM	690, 1.80	625 (611)	-5.09	-3.15	1.95

^aAbsorption edge of film, ^bEstimated optical band-gap from λ_{edge} , ^cMaximum wavelength of polymer in chloroform solution, ^dMaximum wavelength of polymer in solid-state, ^eEstimated from the oxidation onset potential, ^fEstimated from the reduction onset potential.

Cyclic voltammetry (CV) was conducted to investigate the electrochemical properties of the polymers. From the CV measurement, the oxidation onset was obtained and the HOMO energy level was calculated afterwards with the condition

of ferrocene as the energy level reference below the vacuum level. As shown in **Figure III-4**, the HOMO energy level of **PIDT-QxM** and **PIDTT-QxM** are -5.18 and -5.09 eV, respectively. **PIDTT-QxM** indicates the upshifted HOMO level compared to **PIDT-QxM** because of the replacement of two thieno[3,2-b]-thiophene units in IDTT donor [38,58]. While, The LUMO energy level shows the same value of -3.15 eV for both **PIDT-QxM** and **PIDTT-QxM**.

The summary of the energy levels is explained in the **Figure III-5**. Encouraged by this result, it can be concluded that the incorporation of two thieno[3,2-b]thiophene units into the indacenodithiophene moiety and the introduction of electron-donating methoxy into the quinoxaline moiety give the slightly upshifted of HOMO energy level.



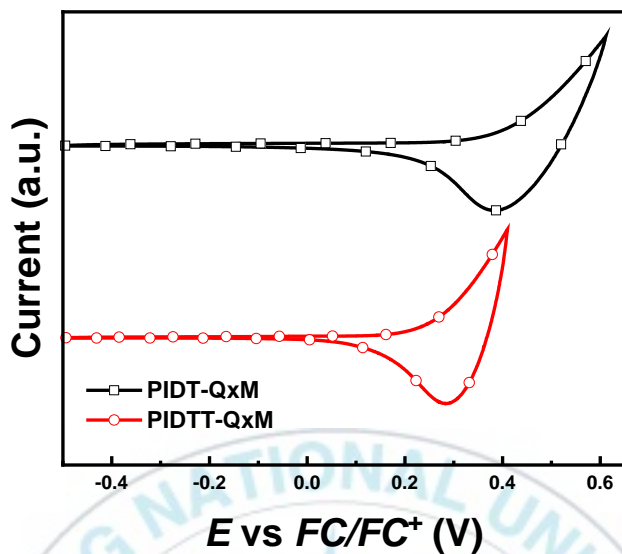


Figure III-4. Cyclic voltammograms of polymers

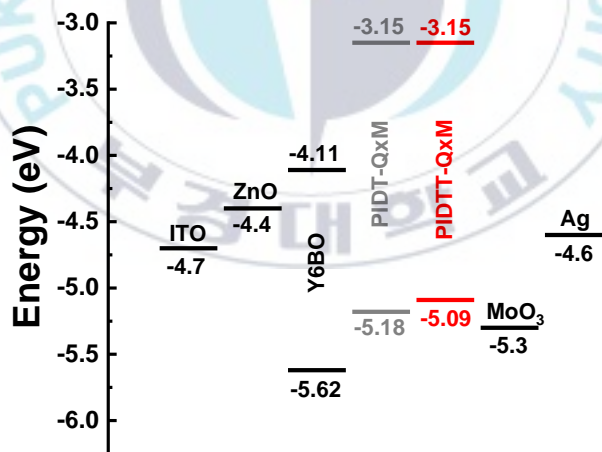


Figure III-5. Energy levels of all polymers in an inverted-type PSCs device

III-2.3. Theoretical Calculations of Polymers

The frontier molecular orbitals and the electronic structures of all polymers were observed using density functional theory (DFT) simulation at the B3LYP/6-311G** level of the Gaussian 09 program. This study was used to understand the theoretical electrochemical properties with the aim to validate the experimental result. For the computational calculation, the hexyl chains on the IDT and IDTT donors were simplified into methyl. While the long polymer chains were represented in only two repeating units of donor-acceptor. As depicted in **Figure III-6**, the distribution of HOMO wave functions of all polymers is localized along the conjugated polymer backbone, while the distribution of LUMO wave function is localized on the electron-withdrawing DPQ unit of the polymer structure. The theoretical HOMO/LUMO energy level of **PIDT-QxM** and **PIDTT-QxM** was -4.46/-2.13 and -4.49/-2.20 eV, resulting in the theoretical bandgap of 2.33 and 2.29 eV, respectively. In addition, **Figure III-7** shows the simulation of molar absorptivity and the electronic transition of polymers. **PIDTT-QxM** exhibited higher molar absorptivity and oscillator strength compared to that **PIDT-QxM** owing to the increased local excitation which is caused by the elongation of conjugation length. These bandgap and molar absorptivity values obtained from the theoretical were in the same trend as the experimental result.

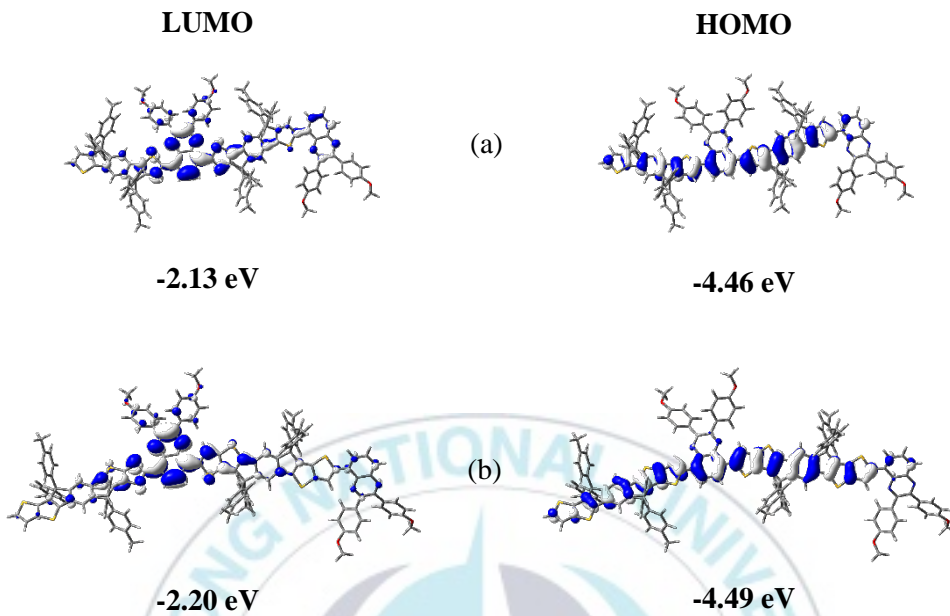


Figure III-6. Frontier molecular orbitals of two-repeating unit models with LUMO and HOMO energy levels calculated at the B3LYP/6-31G** level for (a) PIDT-QxM and (b) PIDTT-QxM

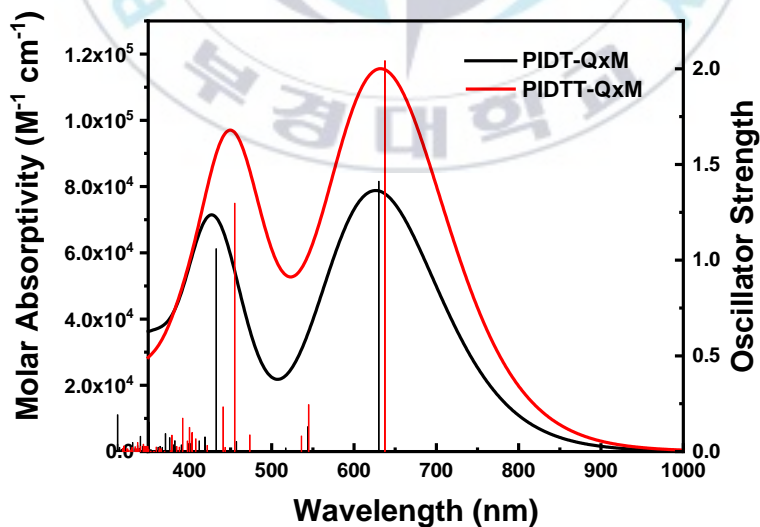


Figure III-7. The Simulation of Molar Absorptivity and Oscillator Strength of Polymer

III-2.4. Photovoltaic Properties of Polymers

The photovoltaic properties of the polymers were evaluated by fabricating an inverted-type PSCs device with the configuration of ITO (15 Ω)/ZnO (25 nm)/active layer (polymer:Y6BO) (105/115 nm)/MoO₃ (3 nm)/Ag (100 nm).

Table III-3. The best photovoltaic parameters of the PSCs. The averages for the photovoltaic parameters of each device are given in parentheses.

Polymer	J_{sc} (mA cm ⁻²)	V_{oc} (V)	FF (%)	PCE (%)	R_s (Ω cm ²) ^a
PIDT-QxM	20.33	0.74	62.1	9.34	2.19
	(20.31)	(0.74)	(61.2)	(9.18)	
PIDTT-QxM	23.35	0.73	61.3	10.40	2.16
	(23.10)	(0.73)	(60.7)	(10.22)	

^aThe series resistance estimated from the corresponding best device.

To optimize the device performance, the blend ratio of donor polymer and acceptor Y6BO in the active layer plays an important role. The proper amount of blend ratio between the donor polymer and acceptor Y6BO is observed by varying the ratio from 3:4 to 3:8 w/w in chloroform solution. The best blend ratios were 3:5 and 3:7 for **PIDT-QxM** and **PIDTT-QxM** with 0.5% v/v of processing additive 1,8-diodooctane (DIO).

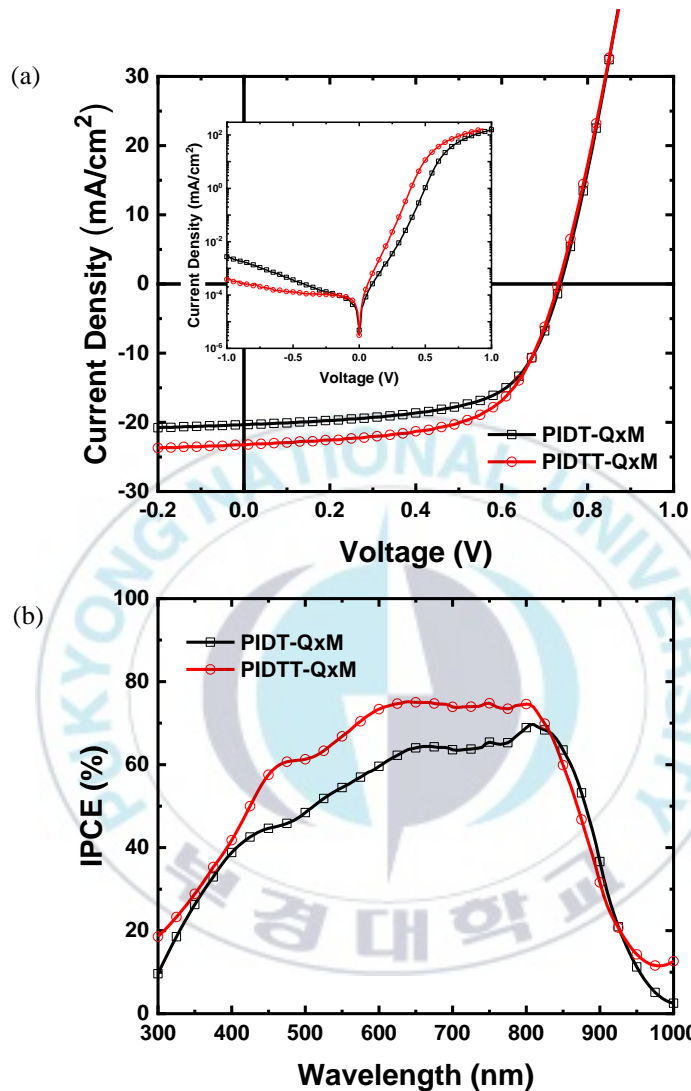
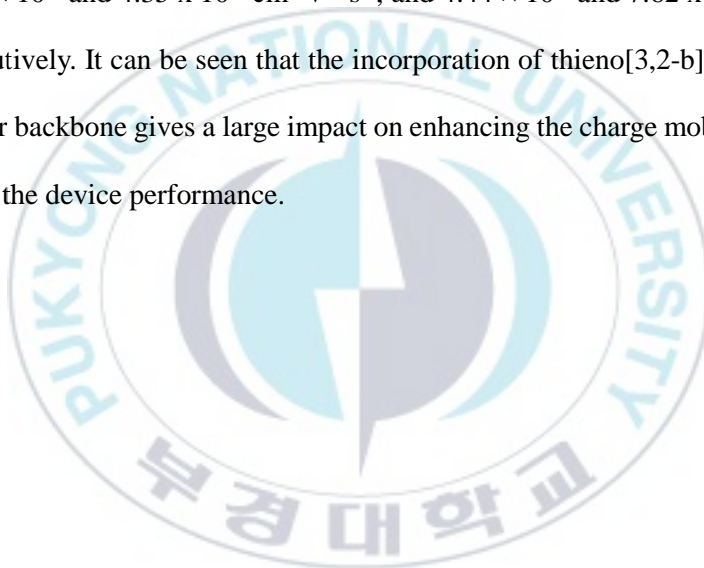


Figure III-8. (a) J-V curve of PSCs under 1.0 sun condition (inset: under the dark condition) and (b) IPCE spectra of PSCs based on PIDT-QxM and PIDTT-QxM.

Figure III-8a shows the current density vs. voltage (J-V) curves of the PSCs device at its optimum condition under AM 1.5G illumination and the detail of the photovoltaic parameters are listed in **Table III-3**. The PCE of PSC device based on **PIDT-QxM** was restricted to 9.34%, while the device based on **PIDTT-QxM** was increased to 10.40%. This obvious improvement in PCE of the device based on **PIDTT-QxM** is corresponding to the higher short circuit current (J_{sc}) of 23.25 mA cm⁻² than that **PIDT-QxM** with 20.33 mA cm⁻² of J_{sc} value. This outcome is in a good agreement with the molar extinction coefficient value. Meanwhile, a decrease of open-circuit voltage (V_{oc}) was noticed in **PIDTT-QxM** (0.73 V) compared to **PIDT-QxM** (0.74 V). This result is in a good accordance with the trend in HOMO energy level. Furthermore, all polymers show the similar value of fill factor (FF) differing around 61-62%.

As illustrated in **Figure III-8b**, all polymers possessed the broad light absorption in the wavelength range of 350 to 900 nm with the maximum incident photon-to-current efficiency (IPCE) value around 70%. This result confirms the UV-Visible absorption spectra and supports the J_{sc} value well. Besides, the inset in **Figure III-8a** explains the J-V curves under the darkness to get the series resistance (R_s) data. **PIDTT-QxM** demonstrated the lower R_s value of 2.16 Ω cm² than that **PIDT-QxM** with the value of 2.19 Ω cm² which is consistent with the overall photovoltaic properties of the devices.

To investigate the charge transporting properties of the polymers, the electron-only and hole-only devices were constructed with the configuration of ITO/ZnO/active layer/LiF/Al and ITO/PEDOT:PSS/active layer/Au, accordingly. **Figure III-9** portrayed that the charge mobility in both polymers show the space charge limited current (SCLC) characteristic corresponding to the popular Mott-Gurney law [59]. The hole and electron mobilities of **PIDT-QxM** and **PIDTT-QxM** were 2.40×10^{-3} and $4.35 \times 10^{-3} \text{ cm}^2 \text{ V}^{-1} \text{ s}^{-1}$, and 4.44×10^{-3} and $7.62 \times 10^{-3} \text{ cm}^2 \text{ V}^{-1} \text{ s}^{-1}$, consecutively. It can be seen that the incorporation of thieno[3,2-b]thiophene in the polymer backbone gives a large impact on enhancing the charge mobilities, thus, optimizing the device performance.



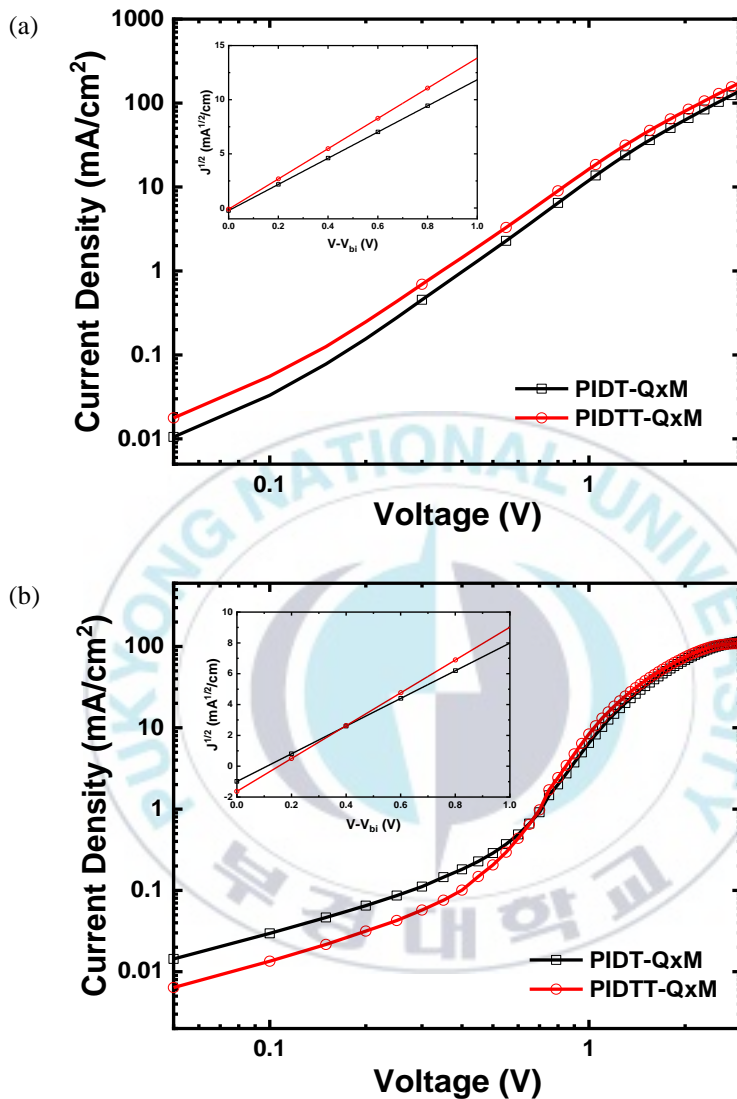


Figure III-9. Current density vs. voltage curves of (a) the electron-only and (b) hole-only devices (inset: current density vs. voltage (V)-built-in voltage (V_{bi}) curves with the fitted line)

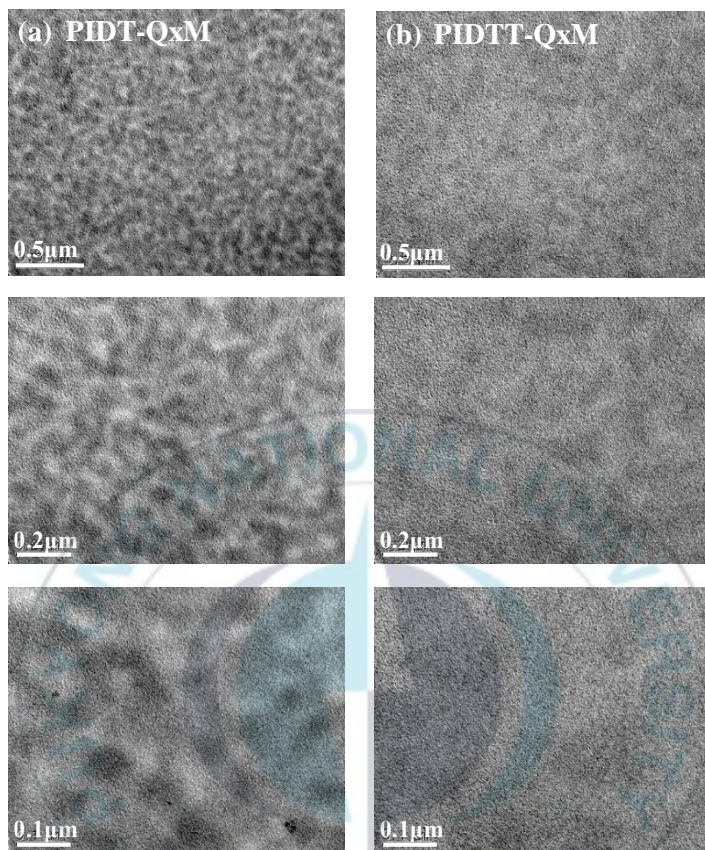


Figure III-10. TEM images of (a) PIDT-QxM and (b) PIDTT-QxM blend film with Y6BO. From top to bottom, the scale bars are 0.5, 0.2, 0.1 μm , respectively.

Figure III-10 presented the transmission electron microscopy (TEM) to know the morphology of all polymer blend films with Y6BO. The more uniform morphology was discovered in **PIDT-QxM** deducing the more complementary blend between polymer and Y6BO rather than that **PIDTT-QxM**. The better microscale phase separation was seen in **PIDTT-QxM** than in **PIDT-QxM**. However, the *FF* value of **PIDT-QxM** is higher than **PIDTT-QxM**. This result shows that *FF* value

is not mainly affected by the morphology, but also the charge-transport properties of the polymers.

III-3. Conclusion

Two D-A type conjugated polymers based on quinoxaline were synthesized via Stille coupling reaction. Methoxy group was introduced to the para position of the phenyl pendants in the side chain of the quinoxaline unit. Then, the electron-donating IDT derivatives (IDT and IDTT) were linked to the same electron-accepting methoxy-substituted quinoxaline moiety to yield **PIDT-QxM** and **PIDTT-QxM**, respectively. These polymers were blended with the Y6BO acceptor in the active layer which further fabricated in the device. The photovoltaic properties exhibited an increase in PCE from 9.34% (**PIDT-QxM**) to 10.40% (**PIDTT-QxM**). This remarkable improvement was attributed to the more planar and extended conjugation length in the polymer backbone by the incorporation of two thieno[3,2-b]thiophene units. The similar value of V_{oc} and FF were observed in both polymers. However, the J_{sc} value was boosted up in **PIDTT-QxM** as the result of the good charge generation. The better morphology was also seen in **PIDTT-QxM**, thus explaining the good charge separation and transport phenomena that support the enhancement in J_{sc} value. After all, this study can offer a comprehensive insight into the utilization of the methoxy group and IDT derivatives in PSCs. A more thorough study is required to maximize other photovoltaic parameters such as V_{oc} and FF with the aim to upgrade the device performance.

Chapter IV. Conclusion

Two series of conjugated polymers were successfully synthesized through Stille coupling reaction. The first series consisted of three polymers whereas IDT derivatives were connected to non-fluorinated and fluorinated DPQ through the thiophene bridge to yield **PIDT-QxMT**, **PIDT-FQxMT**, and **PIDTT-FQxMT**, respectively. An-inverted type device with the structure of ITO/ZnO/active layer/MoO₃/Ag shows that the best performance was obtained by **PIDTT-QxM** with 8.51% of PCE, 22.23 mA cm⁻² of J_{sc} , 0.72 V of V_{oc} , and 52.4% of FF owing to the employment of fluorine substituent and thieno[3,2-b]thiophene units, simultaneously. The second series consisted of two polymers whereas the electron-donating IDT derivatives were directly connected to the simpler electron-accepting methoxy-substituted DPQ to afford **PIDT-QxM** and **PIDTT-QxM**. With the same device configuration, the best performance was found in **PIDTT-QxM** where the PCE was boosted up to 10.40% with 23.25 mA cm⁻² of J_{sc} , 0.73 V of V_{oc} , and 61.3% of FF ascribed to the expanded conjugation length by the presence of dithieno[3,2-b]thiophene.

References

- [1] Graus, W., Blomen, E., and Worrell, E. (2011) Global energy efficiency improvement in the long term: A demand- and supply-side perspective. *Energy Efficiency*. 4 (3), 435–463.
- [2] Gielen, D., Boshell, F., Saygin, D., Bazilian, M.D., Wagner, N., and Gorini, R. (2019) The role of renewable energy in the global energy transformation. *Energy Strategy Reviews*. 24 (June 2018), 38–50.
- [3] York, R. (2016) Decarbonizing the Energy Supply May Increase Energy Demand. *Sociology of Development*. 2 (3), 265–272.
- [4] Kahraman, C., Kaya, I., and Cebi, S. (2009) A comparative analysis for multiattribute selection among renewable energy alternatives using fuzzy axiomatic design and fuzzy analytic hierarchy process. *Energy*. 34 (10), 1603–1616.
- [5] Grätzel, M. (2005) Solar energy conversion by dye-sensitized photovoltaic cells. *Inorganic Chemistry*. 44 (20), 6841–6851.
- [6] (2020) NREL Best-Research-Cell-Efficiencies.pdf.
- [7] Li, C., Liu, M., Pschirer, N.G., Baumgarten, M., and Müllen, K. (2010) Polyphenylene-based materials for organic photovoltaics. *Chemical Reviews*. 110 (11), 6817–6855.

- [8] Li, Y. (2012) Molecular design of photovoltaic materials for polymer solar cells: Toward suitable electronic energy levels and broad absorption. *Accounts of Chemical Research*. 45 (5), 723–733.
- [9] Yao, H., Ye, L., Zhang, H., Li, S., Zhang, S., and Hou, J. (2016) Molecular design of benzodithiophene-based organic photovoltaic materials. *Chemical Reviews*. 116 (12), 7397–7457.
- [10] Shaheen, S.E., Brabec, C.J., Sariciftci, N.S., Padinger, F., Fromherz, T., and Hummelen, J.C. (2001) 2.5% Efficient Organic Plastic Solar Cells. *Applied Physics Letters*. 78 (6), 841–843.
- [11] Paul, H., David, C., and Rand, B.P. (2009) Strategies for increasing the efficiency of heterojunction organic solar cells: Material selection and device architecture. *Accounts of Chemical Research*. 42 (11), 1740–1747.
- [12] Cai, W., Gong, X., and Cao, Y. (2010) Polymer solar cells: Recent development and possible routes for improvement in the performance. *Solar Energy Materials and Solar Cells*. 94 (2), 114–127.
- [13] Yeh, N. and Yeh, P. (2013) Organic solar cells: Their developments and potentials. *Renewable and Sustainable Energy Reviews*. 21 421–431.
- [14] Nicholson, P.G. and Castro, F.A. (2010) Organic photovoltaics: Principles and techniques for nanometre scale characterization.

Nanotechnology. 21 (49),.

- [15] Koster, L.J.A., Shaheen, S.E., and Hummelen, J.C. (2012) Pathways to a new efficiency regime for organic solar cells. *Advanced Energy Materials*. 2 (10), 1246–1253.
- [16] Dimitrov, S.D., Schroeder, B.C., Nielsen, C.B., Bronstein, H., Fei, Z., McCulloch, I., et al. (2016) Singlet exciton lifetimes in conjugated polymer films for organic solar cells. *Polymers*. 8 (1),.
- [17] Terao, Y., Sasabe, H., and Adachi, C. (2007) Correlation of hole mobility, exciton diffusion length, and solar cell characteristics in phthalocyanine/fullerene organic solar cells. *Applied Physics Letters*. 90 (10),.
- [18] . V.K.A. (2014) Organic Solar Cells: Principles, Mechanism and Recent Developments. *International Journal of Research in Engineering and Technology*. 03 (09), 338–341.
- [19] Zhang, F., Xu, X., Tang, W., Zhang, J., Zhuo, Z., Wang, J., et al. (2011) Recent development of the inverted configuration organic solar cells. *Solar Energy Materials and Solar Cells*. 95 (7), 1785–1799.
- [20] Ganesamoorthy, R., Sathiyam, G., and Sakthivel, P. (2017) Review: Fullerene based acceptors for efficient bulk heterojunction organic solar cell applications. *Solar Energy Materials and Solar Cells*. 161

(November 2016), 102–148.

- [21] Jørgensen, M., Norrman, K., and Krebs, F.C. (2008) Stability/degradation of polymer solar cells. *Solar Energy Materials and Solar Cells*. 92 (7), 686–714.
- [22] White, M.S., Olson, D.C., Shaheen, S.E., Kopidakis, N., and Ginley, D.S. (2006) Inverted bulk-heterojunction organic photovoltaic device using a solution-derived ZnO underlayer. *Applied Physics Letters*. 89 (14),.
- [23] Jørgensen, M., Norrman, K., Gevorgyan, S.A., Tromholt, T., Andreasen, B., and Krebs, F.C. (2012) Stability of polymer solar cells. *Advanced Materials*. 24 (5), 580–612.
- [24] Rafique, S., Abdullah, S.M., Sulaiman, K., and Iwamoto, M. (2018) Fundamentals of bulk heterojunction organic solar cells: An overview of stability/degradation issues and strategies for improvement. *Renewable and Sustainable Energy Reviews*. 84 (November 2017), 43–53.
- [25] Arbouch, I., Karzazi, Y., and Hammouti, B. (2014) Organic photovoltaic cells: Operating principles, recent developments and current challenges – review. *Physical and Chemical News*. 72 (4), 73–84.

- [26] Rand, B.P. and Richter, H. (2014) *Organic Solar Cells: Fundamentals, Devices, and Upscaling*. Jenny Stanford Publishing, .
- [27] Padilla, M., Michl, B., Thaidigsmann, B., Warta, W., and Schubert, M.C. (2014) Short-circuit current density mapping for solar cells. *Solar Energy Materials and Solar Cells*. 120 (PART A), 282–288.
- [28] Qi, B. and Wang, J. (2013) Fill factor in organic solar cells. *Physical Chemistry Chemical Physics*. 15 (23), 8972–8982.
- [29] Zheng, Z., Hu, Q., Zhang, S., Zhang, D., Wang, J., Xie, S., et al. (2018) A highly efficient non-fullerene organic solar cell with a fill factor over 0.80 enabled by a fine-tuned hole-transporting layer. *Advanced Materials*. 30 (34), 1–9.
- [30] Huang, Y., Kramer, E.J., Heeger, A.J., and Bazan, G.C. (2014) Bulk heterojunction solar cells: Morphology and performance relationships. *Chemical Reviews*. 114 (14), 7006–7043.
- [31] Lalevée, J. and Fouassier, J.-P. (2015) *Dyes and Chromophores in Polymer Science*. First Edition. 451.
- [32] Mori, D., Benten, H., Okada, I., Ohkita, H., and Ito, S. (2014) Low-bandgap donor/acceptor polymer blend solar cells with efficiency exceeding 4%. *Advanced Energy Materials*. 4 (3), 1–6.
- [33] Jung, J.W., Jo, J.W., Jung, E.H., and Jo, W.H. (2016) Recent progress

in high efficiency polymer solar cells by rational design and energy level tuning of low bandgap copolymers with various electron-withdrawing units. *Organic Electronics*. 31 149–170.

- [34] Brus, V. V., Lee, J., Luginbuhl, B.R., Ko, S.J., Bazan, G.C., and Nguyen, T.Q. (2019) Solution-Processed Semitransparent Organic Photovoltaics: From Molecular Design to Device Performance. *Advanced Materials*. 31 (30), 1–26.
- [35] Li, Y., Gu, M., Pan, Z., Zhang, B., Yang, X., Gu, J., et al. (2017) Indacenodithiophene: A promising building block for high performance polymer solar cells. *Journal of Materials Chemistry A*. 5 (22), 10798–10814.
- [36] Wu, J.S., Cheng, S.W., Cheng, Y.J., and Hsu, C.S. (2015) Donor-acceptor conjugated polymers based on multifused ladder-type arenes for organic solar cells. *Chemical Society Reviews*. 44 (5), 1113–1154.
- [37] McCulloch, I., Ashraf, R.S., Biniek, L., Bronstein, H., Combe, C., Donaghey, J.E., et al. (2012) Design of semiconducting indacenodithiophene polymers for high performance transistors and solar cells. *Accounts of Chemical Research*. 45 (5), 714–722.
- [38] Xu, Y.X., Chueh, C.C., Yip, H.L., Ding, F.Z., Li, Y.X., Li, C.Z., et al. (2012) Improved charge transport and absorption coefficient in

- indacenodithieno[3,2-b]thiophene-based ladder-type polymer leading to highly efficient polymer solar cells. *Advanced Materials*. 24 (47), 6356–6361.
- [39] Antoniotti, S. and Duñach, E. (2002) Direct and catalytic synthesis of quinoxaline derivatives from epoxides and ene-1,2-diamines. *Tetrahedron Letters*. 43 (22), 3971–3973.
- [40] Gedefaw, D., Prosa, M., Bolognesi, M., Seri, M., and Andersson, M.R. (2017) Recent Development of Quinoxaline Based Polymers/Small Molecules for Organic Photovoltaics. *Advanced Energy Materials*. 7 (21),.
- [41] Li, S., Ye, L., Zhao, W., Zhang, S., Ade, H., and Hou, J. (2017) Significant Influence of the Methoxyl Substitution Position on Optoelectronic Properties and Molecular Packing of Small-Molecule Electron Acceptors for Photovoltaic Cells. *Advanced Energy Materials*. 7 (17),.
- [42] Tan, Z., Zhou, E., Yang, Y., He, Y., Yang, C., and Li, Y. (2007) Synthesis, characterization and photovoltaic properties of thiophene copolymers containing conjugated side-chain. *European Polymer Journal*. 43 (3), 855–861.
- [43] Lin, H., Chen, S., Li, Z., Lai, J.Y.L., Yang, G., McAfee, T., et al. (2015)

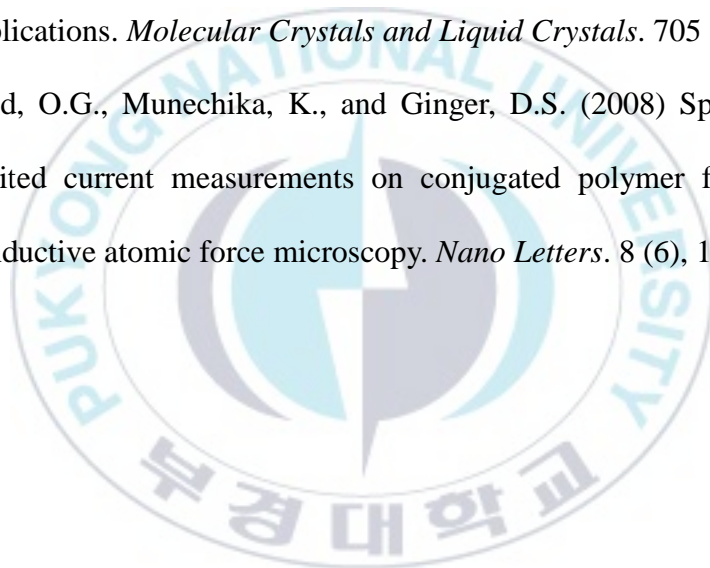
- High-Performance Non-Fullerene Polymer Solar Cells Based on a Pair of Donor-Acceptor Materials with Complementary Absorption Properties. *Advanced Materials*. 27 (45), 7299–7304.
- [44] Putri, S.K., Kim, Y.H., Whang, D.R., Lee, M.S., Kim, J.H., and Chang, D.W. (2017) Step-by-step improvement in photovoltaic properties of fluorinated quinoxaline-based low-band-gap polymers. *Organic Electronics: Physics, Materials, Applications*. 47 14–23.
- [45] Liao, L., Dai, L., Smith, A., Durstock, M., Lu, J., Ding, J., et al. (2007) Photovoltaic-active dithienosilole-containing polymers. *Macromolecules*. 40 (26), 9406–9412.
- [46] Kim, J., Yun, M.H., Kim, G.H., Lee, J., Lee, S.M., Ko, S.J., et al. (2014) Synthesis of PCDTBT-based fluorinated polymers for high open-circuit voltage in organic photovoltaics: Towards an understanding of relationships between polymer energy levels engineering and ideal morphology control. *ACS Applied Materials and Interfaces*. 6 (10), 7523–7534.
- [47] Chochos, C.L., Singh, R., Kim, M., Gasparini, N., Katsouras, A., Kulshreshtha, C., et al. (2016) Enhancement of the Power Conversion Efficiency in Organic Photovoltaics by Unveiling the Appropriate Polymer Backbone Enlargement Approach. *Advanced Functional*

Materials. 26 (11), 1840–1848.

- [48] Chochos, C.L., Singh, R., Gregoriou, V.G., Kim, M., Katsouras, A., Serpetzoglou, E., et al. (2018) Enhancement of the Power-Conversion Efficiency of Organic Solar Cells via Unveiling an Appropriate Rational Design Strategy in Indacenodithiophene-*alt*-quinoxaline π -Conjugated Polymers. *ACS Applied Materials and Interfaces*. 10 (12), 10236–10245.
- [49] Price, S.C., Stuart, A.C., Yang, L., Zhou, H., and You, W. (2011) Fluorine substituted conjugated polymer of medium band gap yields 7% efficiency in polymer-fullerene solar cells. *Journal of the American Chemical Society*. 133 (12), 4625–4631.
- [50] Dang, D., Chen, W., Himmelberger, S., Tao, Q., Lundin, A., Yang, R., et al. (2014) Enhanced Photovoltaic Performance of Indacenodithiophene-Quinoxaline Copolymers by Side-Chain Modulation. *Advanced Energy Materials*. 4 (15), 1–5.
- [51] Zhou, H., Yang, L., Stuart, A.C., Price, S.C., Liu, S., and You, W. (2011) Development of Fluorinated Benzothiadiazole as a Structural Unit for a Polymer Solar Cell of 7 % Efficiency. *Angewandte Chemie*. 123 (13), 3051–3054.
- [52] Xu, X., Li, Z., Bäcke, O., Bini, K., James, D.I., Olsson, E., et al. (2014)

- Effects of side chain isomerism on the physical and photovoltaic properties of indacenodithieno[3,2-b]thiophene-quinoxaline copolymers: Toward a side chain design for enhanced photovoltaic performance. *Journal of Materials Chemistry A*. 2 (44), 18988–18997.
- [53] Röhr, J.A., Moia, D., Haque, S.A., Kirchartz, T., and Nelson, J. (2018) Exploring the validity and limitations of the Mott-Gurney law for charge-carrier mobility determination of semiconducting thin-films. *Journal of Physics Condensed Matter*. 30 (10),.
- [54] Zalar, P., Kuik, M., Ran, N.A., Love, J.A., and Nguyen, T.Q. (2014) Effects of processing conditions on the recombination reduction in small molecule bulk heterojunction solar cells. *Advanced Energy Materials*. 4 (14), 1–7.
- [55] Kim, J.H., Shin, S.A., Park, J.B., Song, C.E., Shin, W.S., Yang, H., et al. (2014) Fluorinated benzoselenadiazole-based low-band-gap polymers for high efficiency inverted single and tandem organic photovoltaic cells. *Macromolecules*. 47 (5), 1613–1622.
- [56] Handoko, S.L., Jin, H.C., Whang, D.R., Putri, S.K., Kim, J.H., and Chang, D.W. (2019) Synthesis of quinoxaline-based polymers with multiple electron-withdrawing groups for polymer solar cells. *Journal of Industrial and Engineering Chemistry*. 73 192–197.

- [57] Handoko, S.L., Jin, H.C., Whang, D.R., Kim, J.H., and Chang, D.W. (2020) Effect of cyano substituent on photovoltaic properties of quinoxaline-based polymers. *Journal of Industrial and Engineering Chemistry*. 86 244–250.
- [58] Wardani, R.P., Jin, H.C., Kim, J.H., and Chang, D.W. (2020) Synthesis of quinoxaline-based D-A type conjugated polymers for photovoltaic applications. *Molecular Crystals and Liquid Crystals*. 705 (1), 15–21.
- [59] Reid, O.G., Munechika, K., and Ginger, D.S. (2008) Space charge limited current measurements on conjugated polymer films using conductive atomic force microscopy. *Nano Letters*. 8 (6), 1602–1609.



Acknowledgements

Alhamdulillahirabbil' alamin.

I am sincerely grateful to my advisor, Professor Dong Wook Chang, for his supervision during my study in Functional Polymer Laboratory. I also would like to thank Professor Joo Hyun Kim, Ho Cheol, and Mi Jin, who help me with the device fabrication. My best regard goes to Professor Min Young Shon and Professor Young Eup Jin, as well, for being the committee members of my defense. Not to be forgotten, to other professors and officers in Industrial Chemistry Department that help and assist me.

My study period here was filled with ups and downs. To Mbak Shinta, thank you for being fast-response whenever I contact you. To Mbak Gita, thank you for guiding me at the beginning of my study, bearing with me throughout the process, and even listening to my story at nearly the end of my study. To Mun Ho and Jun Tae, thank you for being the first Korean friends I've ever made. To my labmate, Seok Woo, thank you for your help, kindness, and for being the one I can lean on in my last year of study. To Ye Ji, Ji Min, and Eun Young, I cherish our short moments together.

To my parents, thank you for always putting my name in your prayer and encouraging me to be a tough girl whenever I feel depressed. To Mbak Diah and Aifa, thank you for enlightening our family group chat. It cheers me up.

To Mas Irwan, thank you for always being there for me, for making me laugh and comforting me whenever I have a bad day, for supporting my decisions, and helping me with my thesis defense preparation. I wish you good luck in pursuing your Ph.D. To Mbak Merreta, thank you for being that *gaspol*-person to make our crazy ideas happen. To Mbak Intan, Mbak Sabrina, Mbak Ace, Mbak Moli, Mbak Ratna, Mbak Dea, Mbak Sonita, Ilham, Rai, Miko, Boi, and all my Indonesian friends here, thank you for our memories together. I hope the best for your future endeavors.

To Mas Pundhi, thank you for convincing me to take this path. To my other friends in Indonesia, Mbak Sarah, Alda, Istiq, Claudya, Yulius, Dany, Rama, Aldo, and all *K54* and *FACT* companions, as time goes by our priority may change, but thank you for being in touch. I wish you all keep being healthy despite this pandemic.